

The Nico Pérez terrane (Uruguay) and its archean and paleoproterozoic inheritance

*Leda Sánchez Bettucci¹, Umberto Cordani², Judith Loureiro³, Elena Peel¹, Santiago Fort¹, Kei Sato²

¹Universidad de la República, Facultad de Ciencias, Iguá 4225 esquina Mataojo, Montevideo, 11400 Uruguay.

leda@fcien.edu.uy; sfort@fcien.edu.uy; elena@fcien.edu.uy

²Instituto de Geociências-Universidade de São Paulo, R. do Lago, 562-Butantã, SP, 05508-080, Brasil.

ucordani@usp.br; keisato@usp.br

³Dirección Nacional de Minería y Geología-MIEM Hervideo 2861, Montevideo, Uruguay.

Judith.Loureiro@miem.gub.uy

* Corresponding author: leda@fcien.edu.uy

ABSTRACT. A U-Pb SHRIMP zircon geochronological study was carried out in the Nico Pérez Terrane in the central-eastern portion of Uruguay with the aim of constraining its geological evolution and its cratonic affinity. Nico Pérez Terrane is made up by a mosaic of tectonic blocks with different lithologies and sizes. This terrane is limited to the west by the Piedra Alta Terrane through the Sarandí del Yí shear zone, and to the east, is in tectonic contact through the Retamosa thrust with the Dom Feliciano Belt (Brasiliano orogenic cycle). Lithologically, the Nico Pérez Terrane is composed by medium to high grade metamorphic rock contained in three tectonic blocks (Pavas, Valentines and Rivera blocks) represented mainly by granitoids, as well as ortho and parametamorphic rocks, such as amphibolites, metapyroxenites, BIFs, schists, quartzites with fuchsite, among others. Archean inheritance, Rhyacian, Statherian, and Neoproterozoic magmatic ages are reported here. Similar ages, which show Archaean inheritance and Neoproterozoic imprint, reported in units of the Piedra Alta Terrane modify the idea that the Río de La Plata Craton only corresponds to a juvenile Paleoproterozoic tectonic unit. This, together with recently published geophysical information, supports the cratonic affinity of the Nico Pérez Terrane with the Río de La Plata Craton.

Keywords: Nico Pérez Terrane, Río de La Plata Craton, Archean inliers, U-Pb SHRIMP zircon ages.

RESUMEN. El terreno Nico-Pérez (Uruguay) y su herencia arcaica y paleoproterozoica. Un estudio geocronológico U-Pb SHRIMP en circon fue realizado en rocas del Terreno Nico Pérez, con el objetivo de circunscribir la evolución geológica y su afinidad cratónica. Este terreno, localizado en la porción central del Uruguay, está constituido por un mosaico de tres bloques tectónicos y se encuentra limitado al oeste por el Terreno Piedra Alta a través de la zona de cizallamiento Sarandí del Yí. Al este, se encuentra en contacto tectónico a través del corrimiento Retamosa con el Cinturón Dom Feliciano (Ciclo Orogénico Brasiliano). Litológicamente, el Terreno Nico Pérez está compuesto por rocas metamórficas de grado medio a alto (bloques Pavas, Valentines y Rivera) representados principalmente por granitoides, así como por rocas orto- y parametamórficas, tales como anfibolitas, metapiroxenitas, BIFs, esquistos, cuarcitas con fucsita, entre otras. Se presenta en este trabajo un conjunto de edades magmáticas que poseen herencia arqueana, y edades riacianas, estaterianas y neoproterozoicas. Edades similares a estas, que muestran herencia arqueana e impronta neoproterozoica, reportadas en unidades del Terreno Piedra Alta, modifican la idea de que el Cratón del Río de La Plata corresponde a una unidad tectónica paleoproterozoica juvenil. Esto, junto con la información geofísica publicada recientemente, respalda la afinidad cratónica del Terreno Nico Pérez con el Cratón del Río de La Plata.

Palabras clave: Terreno Nico Pérez, Cratón del Río de La Plata, Inliers arqueanos, Edades U-Pb SHRIMP.

1. Introduction

The Nico Pérez Terrane, located in the central portion of Uruguay (Fig. 1), records the oldest basement ages of the region. Bossi and Campal (1992) identified this terrane from the main outcropping areas of the Río de La Plata Craton (*sensu* Almeida *et al.*, 1973) and based on lithological and structural

data they defined it as a Paleoproterozoic block affected by tectono-magmatic events related to the Brasiliano-Panafrican orogenic cycle. Additionally, these authors postulated that the Nico Pérez Terrane represents the foreland of the Neoproterozoic orogenic belt known as Dom Feliciano Belt (Fragoso-César, 1980). Later works by Hartmann *et al.* (2001), Santos *et al.* (2003), Mallmann *et al.* (2007), Gaucher

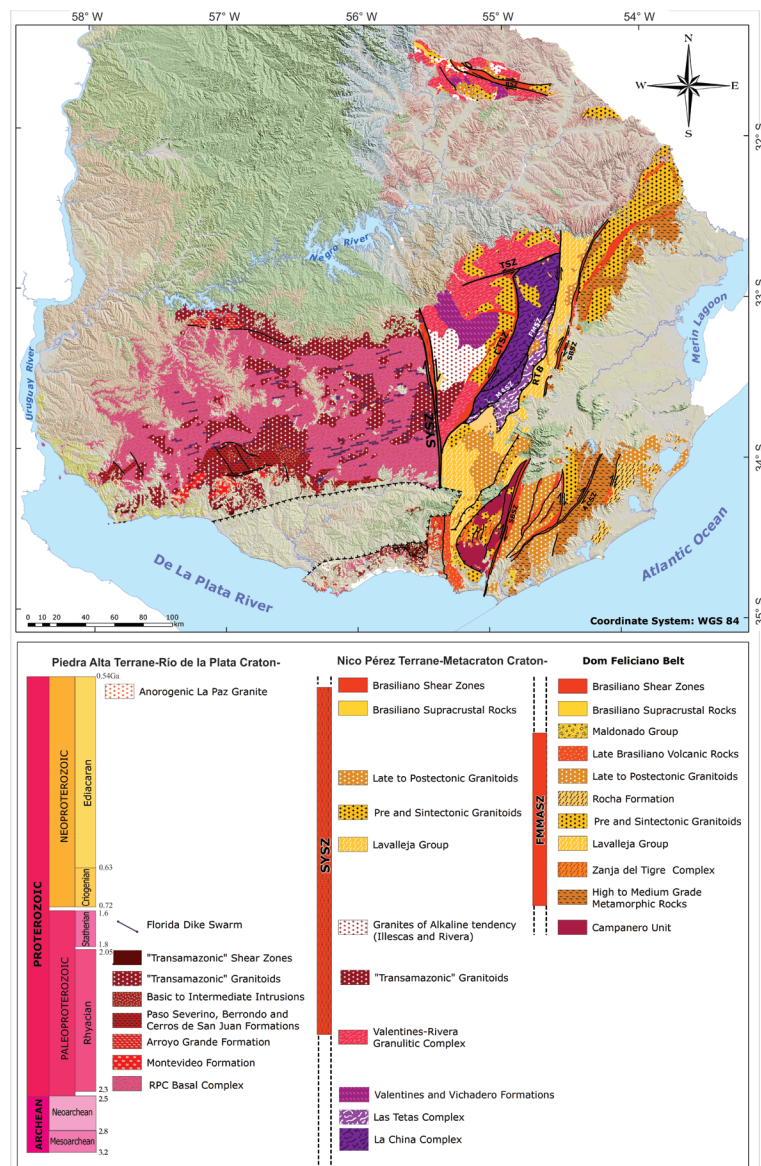


FIG. 1. Geologic map from Uruguay showing the basement most conspicuous units. **SYSZ**: Sarandí del Yi shear zone; **FMSZ**: Fraile Muerto shear zone; **MASZ**: María Albina shear zone; **CTSZ**: Cueva del Tigre shear zone; **RT**: Retamosa thrust; **TSZ**: Tupambaé shear zone; **RSZ**: Rivera shear zone; **SBSZ**: Sierra Ballena shear zone; **ACSZ**: Alférrez-Cordillera shear zone. (Modified from Loureiro *et al.*, 2019).

et al. (2010a), Oyhantçabal *et al.* (2012, 2018) and Oriolo *et al.* (2016a), among others, allowed the recognition of Archean and Paleoproterozoic basement rocks and the intense impact of Neoproterozoic granitic intrusions and deformation in the Nico Pérez terrane. Additionally, several authors (*e.g.*, Bossi *et al.*, 1998; Hartmann *et al.*, 2001; Bossi and Gaucher, 2004; Mallmann *et al.*, 2007; Gaucher *et al.*, 2010 (a, b); Oriolo *et al.*, 2016a; Oyhantçabal

et al., 2018) have extended its eastern border to the Sierra Ballena shear zone (Fig. 2). Oyhantçabal *et al.* (2011) challenged its affinity with the Río de la Plata Craton based on lithologic, structural, geochronologic, and isotopic data. Recently, Oriolo *et al.* (2016a, 2017) interpreted this terrane as a basement inlier of the Dom Feliciano Belt, and they suggested its affinity with the West Africa Congo Craton based on tectonostratigraphy, U-Pb ages, and Hf isotopic data.

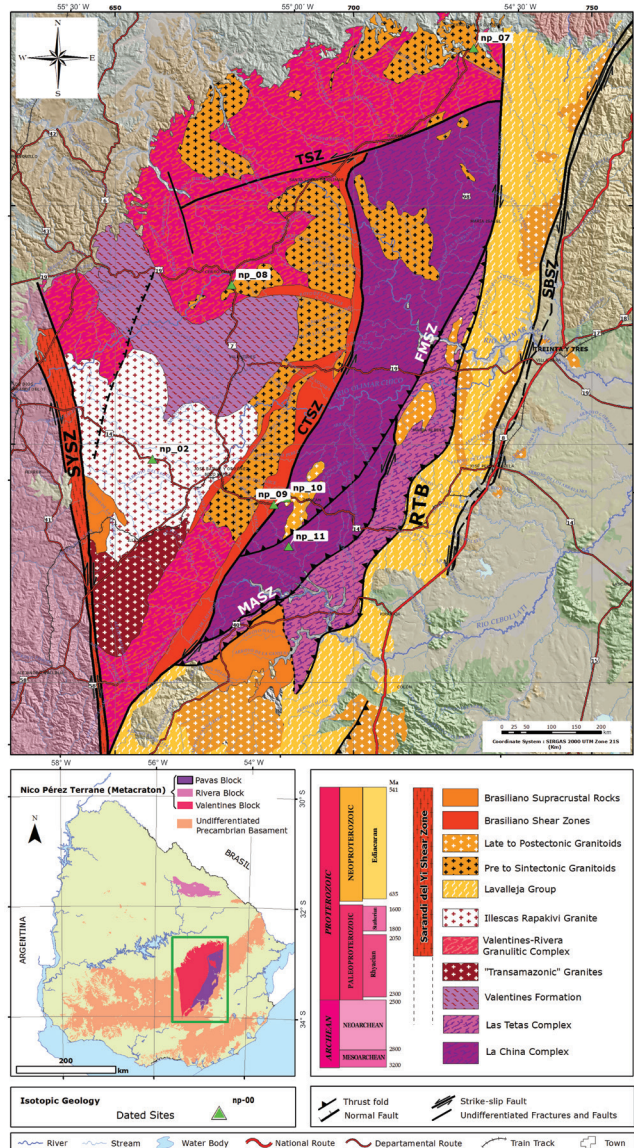


FIG 2. Geologic map of the Valentines and Pavas Blocks (Nico Pérez Terrane) showing dated points. **SYSZ:** Sarandí del Yí shear zone; **FMSZ:** Fraile Muerto shear zone; **MASZ:** María Albina shear zone; **CTSZ:** Cueva del Tigre shear zone; **RT:** Retamosa thrust; **TSZ:** Tupambaé shear zone; **SBSZ:** Sierra Ballena shear zone. Modified from Loureiro *et al.* (2019).

After almost 30 years since its original definition, the Nico Pérez Terrane is considered an Archean-Paleoproterozoic crustal block with Neoproterozoic reworking related to the Brasiliano Orogeny, even though its affinity with the Río de la Plata Craton and its limits are still being subjects of controversy (e.g., Sánchez Bettucci *et al.*, 2010a; Santos *et al.*, 2019; Oyhantçabal *et al.*, 2018; Bologna *et al.*, 2019; Loureiro *et al.*, 2019). In this paper, new SHRIMP U-Pb zircon ages from rocks of nine samples from six sites (see Fig. 2) are presented. These ages are integrated with geological, geophysical, and geochronological evidence to provide constraints for the understanding of the geological evolution of the Uruguayan basement. Also, an appraisal about the limits and the affinity of the Nico Pérez Terrane with the Congo or Río de La Plata cratons are presented based on available information.

2. Geological framework of the Nico Pérez Terrane

The Nico Pérez terrane is located between the Sarandí del Yí shear zone to the west and the Retamosa thrust (RT) to the east and south (Fig. 1). Its northeastern limit is along the Fraile Muerto shear zone. Both, the Retamosa thrust and Fraile Muerto shear zone separate it from the supracrustal sequence of the Dom Feliciano Belt (e.g., Bossi and Campal, 1992; Sánchez Bettucci *et al.*, 2010b). Meanwhile, the Sarandí del Yí shear zone separates the Nico Pérez Terrane from the Piedra Alta Terrane developed to the west. The Piedra Alta Terrane (Bossi *et al.*, 1993) includes low to medium metamorphic orogenic belts (*ca.* 2.1 Ga), a layered mafic complex, a gneissic-migmatitic basement, pre- to syn- orogenic granitoids, mafic and felsic late to post orogenic magmatism (1.9-2.3 Ga), A-type rapakivi granites (2.078 Ga), and extensional magmatism (1.7 Ga) represented by a mafic dike swarm (Sánchez Bettucci *et al.*, 2010a; Franceschinis *et al.*, 2019 and references therein). All these lithostratigraphic units were assigned to the Transamazonian orogenic cycle (Hurley *et al.*, 1967; Choubert and Faure-Muret, 1969; Almeida *et al.*, 1973) or Transplatense orogenic cycle (Santos *et al.*, 2019).

From Almeida *et al.* (1973) the current areas of the Nico Pérez Terrane and Piedra Alta Terrane have been considered a part of the Río de la Plata Craton. The Río de La Plata Craton (*sensu* Almeida *et al.*, 1973) occupies approximately the third part

of the south-western region of Uruguay (Fig. 1). It extends towards the north of the country in Rivera and Aceguá (near the Brazilian border), and crops out in Brazil, at the eastern part of Rio Grande do Sul State (Taquarembó and Encruzilhada terranes). Also, it crops out in the Tandil mountain ranges in Argentina. Oyhantçabal *et al.* (2011) questioned this concept in a review of the Río de La Plata Craton. These authors based on features like Sm/Nd T_{DM} model ages (Piedra Alta Terrane T_{DM} 2.8-2.3 Ga; Nico Pérez Terrane T_{DM} 3.0-2.6 and 2.3-1.6 Ga), crystallization ages (Piedra Alta Terrane 2.2-2.1 Ga; Nico Pérez Terrane 3.1-0.57 Ga), and differences in gravity signature for both terranes, proposed that the Nico Pérez Terrane and Taquarembo block are allochthonous to the Río de La Plata Craton, comprising only the Piedra Alta and Tandilia terranes. However, Santos *et al.* (2017) reported for the first time Archean inheritance (T_{DM} Hf: 2.52 Ga; average ϵ_{Hf} : 3.62) and Brasiliano reworking in the Piedra Alta Terrane, modifying the established idea of only Rhyacian juvenile crust. Besides, Bologna *et al.* (2019) based on a magnetotelluric study of the Piedra Alta and Nico Pérez terranes mentioned that their results showed no lithospheric-scale contrast in the electrical resistivity across the Sarandí del Yí shear zone. In addition, they suggested the Nico Pérez Terrane is the remobilized metacratic portion (*sensu* Liégeois *et al.*, 2013) of the Río de La Plata Craton, as previously suggested by Santos *et al.* (2019). Regional syntheses of the tectonic evolution of the Río de La Plata Craton in Uruguay are available in Rapela *et al.* (2007); Sánchez Bettucci *et al.* (2010a); Oyhantçabal *et al.* (2011, 2018); Cingolani *et al.* (2012); Santos *et al.* (2019); Bologna *et al.* (2019) and references therein.

As stated above, the Nico Pérez Terrane is made up of Archean and Paleoproterozoic high-grade metamorphic sequences and granitoid rocks, as well as post-orogenic magmatic rocks. It comprises the Pavas, Valentines, Rivera and Aceguá structural blocks, as shown in figures 1 and 2. The main features of each of these structural blocks are presented below.

2.1. Pavas Block

The Pavas Block (*sensu* Preciozzi *et al.*, 1985) is composed by La China and Las Tetas Archean complexes (Hartmann *et al.*, 2001), covering approximately 2,025 km² and 635 km², respectively

(Loureiro *et al.*, 2019), both with an NE-SW regional structural trend. To the north and west, La China Complex is in tectonic contact with the Valentines Block through Cueva del Tigre shear zone. To the south-east this complex thrusts Las Tetas Complex by the María Albina shear zone, and to the north-east, it is in tectonic contact with the supracrustal rocks of the Dom Feliciano Belt by the Fraile Muerto shear zone (see Fig. 2).

La China Complex is described as a set of orthogneisses, granitoids, and a greenstone belt consisting of igneous mafic and ultramafic rocks with subordinate cherts, that underwent significant deformation and metamorphism under amphibolite facies conditions; also it contains a few Neoproterozoic intrusions. The complex presents a general composition of tonalite-trondhjemite-granodiorite (TTG) according to Hartmann *et al.* (2001). The protoliths of the metaultramafic rocks have been interpreted as hzzburgites, dunites and komatiites. Serpentinites, talc-chlorite-tremolite schists and amphibolites are

common (Preciozzi *et al.*, 1979, 1985; Hartmann *et al.*, 2001; Gaucher *et al.*, 2014a, b). Metatonalites are the rocks where most of the Archean ages have been reported. They present irregular compositional bands, with amphibole and quartz-feldspathic rich bands (Fig. 3). The Zapicán diorite intrudes the La China Complex, and crops out as NNE-SSW body (Lossada *et al.*, 2014). It comprises diorites to granodiorites, often containing hornblende and gabbroic enclaves (Fig. 3).

Las Tetas Complex is defined as a succession of metasedimentary rocks affected by amphibolite facies metamorphism, consisting of meta-quartzites with fuchsite, metaconglomerates, micaschists with staurolite and garnet, gneisses with muscovite and tourmaline, BIFs and dolomitic marbles (Hartmann *et al.*, 2001; Masquelin *et al.*, 2017; and references therein). This complex has a decreasing metamorphic grade from north to south (Gaucher *et al.*, 2014a; Oyhantçabal *et al.*, 2018) from quartzites with sillimanite in the north, to micaceous shales with

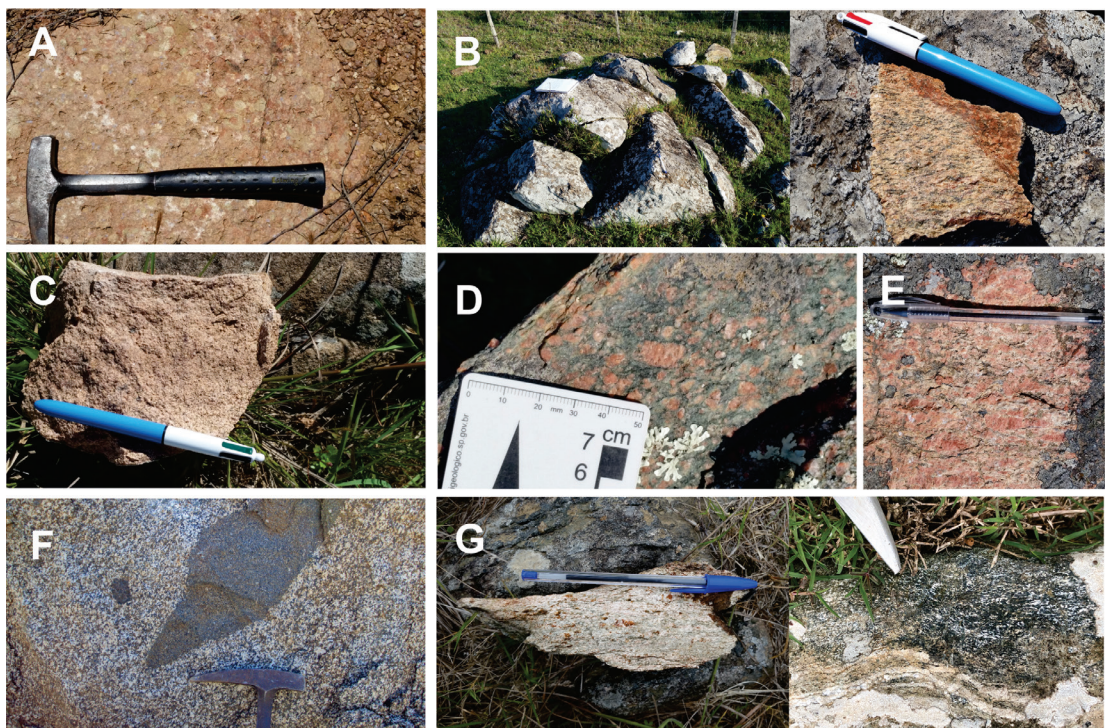


FIG. 3. A. General view of Illescas rapakivi granite (sample NP-02); B. General view of foliated granitoid (sample NP-07) at the Cerro de las Cuentas; C. Cerro Chato granite (sample NP-08); D. Mylonitic granite inside the Cueva del Tigre shear zone (NP-09A); recrystallized granite; E. Foliated granitoid (NP-09B); F. Deformed Zapicán diorite (NP-10); G. Foliated leucogranite of the La China Complex (NP-11) that shows irregular compositional bands, with amphibole and quartz-feldspathic rich bands.

staurolite and garnet in the south (Hartmann *et al.*, 2001). According to Oyhantçabal *et al.* (2018) and Loureiro *et al.* (2019), along its southeastern limit, represented by the Retamosa thrust (this work), the unit presents small flakes intercalated with supracrustal rocks of the Dom Feliciano Belt.

2.2. Valentines Block

The Valentines Block (Preciozzi *et al.*, 1979) is located between the Sarandí del Yí shear zone and the Cueva del Tigre shear zone, next to the Pavas Block (Fig. 2). It is characterized by metatradnjemites, metagranites and metatonalites. Ferriferous conglomerates, magnetite-rich quartzites, banded magneto-augite quartzites, BIFs, also cherts have been described, as well as amphibolites, pyroxenites, garnet-pyroxene quartzites and forsterite-diopside marbles (*e.g.*, Bossi and Umpierre, 1969; Masquelin, 2006; Oyhantçabal *et al.*, 2011; Oriolo *et al.*, 2016a). The Valentines Block is constituted by the Valentines-Rivera Granulitic Complex (Oyhantçabal *et al.*, 2011), and a few Proterozoic igneous intrusions. Lithologically, the Valentines-Rivera Granulitic Complex is composed mainly by granulitic gneisses, para-gneisses, meta-pyroxenites, magnetite-augite quartzites, meta-tonalites, metatradnjemites, migmatites, among others (Mallmann *et al.*, 2007; Oyhantçabal *et al.*, 2011 and references therein). The supracrustal rocks (paragneisses, quartzites, BIF) of this complex are included in the Valentines Formation (Bossi *et al.*, 1965). The granulites are correlated and grouped with similar rocks from Brazil in the Taquarembó Block (Hartmann *et al.*, 1999; Oyhantçabal *et al.*, 2011; and references therein) and with the Santa María Chico Complex in Rio Grande do Sul (Massonne *et al.*, 2001; and references therein).

Within this block, Campal and Schipilov (1995) described the occurrence of a large A-type rapakivi granite (Illescas Batholith, Fig. 3). It has a coarse- to medium-grain texture, with K-feldspar, plagioclase, quartz, amphibole, and biotite. It presents ductile deformation in its borders and it is cut by Sarandí del Yí shear zone (Campal and Schipilov, 1995). Gaucher and Blanco (2014) based on few and partial geochemical data suggested a within plate tectonic environment. On the contrary, Oriolo *et al.* (2019) conducted a geochemical study concluding that the Illescas granite exhibits meta- to peraluminous nature

with dominant shoshonitic and ferroan composition, suggesting a post-collisional/post-orogenic setting.

2.3. Rivera Block

The Rivera Block (Preciozzi *et al.*, 1979) is in the northeastern portion of Uruguay (Figs. 1 and 4) and is an isolated block surrounded by Palaeozoic sedimentary rocks from the Paraná Basin. The basement is a bimodal felsic-mafic association that underwent high-grade metamorphism constituted by granulitic othogneisses and subordinate orthopyroxene and garnet-bearing mafic granulites, grouped by Oyhantçabal *et al.* (2012) in the Valentines-Rivera Granulitic Complex. The regional structural trend is EW, affected by ductile shear zones (Fig. 4), attributed originally to the Brasiliano orogeny by Cordani and Soliani (1990).

In addition, the rocks of the Vichadero Formation are interlayered with the Valentines-Rivera Granulitic Complex (Oyhantçabal *et al.*, 2012). This formation is composed of pyroxene fels, sillimanite gneisses, quartzites, forsterite marbles, metabasites, BIFs, calc-silicate rocks, and manganese-formations (Ellis De Luca, 1998). Important ore deposits (gold) occur related to the regional structural trend.

2.4. Neoproterozoic cover rocks, granitic plutons, and shear zones

In the Valentines Block, the Neoproterozoic cover is represented by the Cerro San Francisco and Cerros Victoria Formations, made up by meta-sandstones and meta-subarkoses, and by the oolitic and stromatolitic meta-limestone with low metamorphic grade, respectively, deposited in restricted sedimentary basin (Montaña and Sprechmann, 1993). In the Rivera Block, some outcrops of low-grade metamorphic rocks are described (*e.g.*, Preciozzi *et al.*, 1985; Gaucher, 2000).

An important Neoproterozoic magmatism, related to the Brasiliano orogenic cycle, crops out all over the Nico Pérez Terrane (Preciozzi *et al.*, 1979; Cordani and Soliani, 1990; Oyhantçabal *et al.*, 2012; Oriolo *et al.*, 2016a; among others). Foliated granitic plutons occupy about 30% of the area covered by the Nico Pérez Terrane (Fig. 2). The granitoids are syn-, late-, to post-orogenic and they are coupled with the regional structures with NE-SW trends related to the Brasiliano Orogeny. Two of them, the Cerro

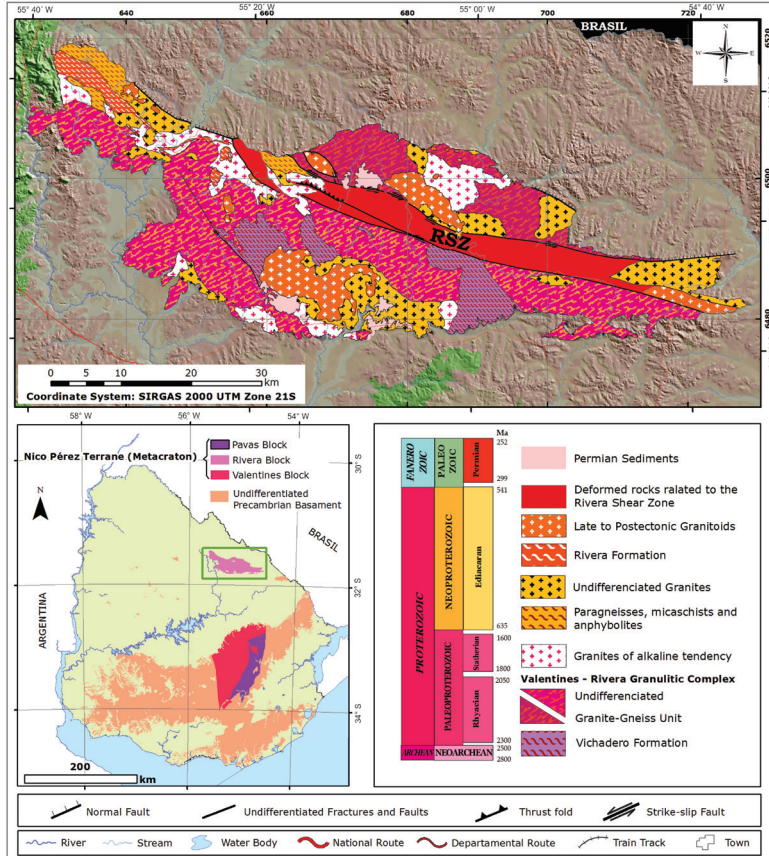


FIG. 4. Rivera Block geological map, modified from Loureiro (2008).

de las Cuentas and the Cerro Chato granites (Fig. 3), are studied in this work (see Section 4).

The most important shear zone that affects the Nico Pérez Terrane is the Paleoproterozoic Sarandí del Yí shear zone (Fig. 1). It comprises up to 13 km wide and more than 250 km long in the north-south direction (Gómez Rifas, 1989). Preciozzi *et al.* (1979) were the first to recognize this feature, with a N10° structural trend developed between the Sarandí of Yí town (Durazno department) and the Sierra de Las Ánimas Complex (Fig. 1). Bossi and Campal (1992) described it as a dextral megashear zone, based on features like the Florida dike swarm flexure, which are clearly well defined in the aerogeophysical survey (Dinamige, 2016). Oyhantçabal *et al.* (1993) suggested that this shear zone was reactivated with a sinistral sense during the Brasiliano orogenic cycle. Furthermore, Oriolo *et al.* (2016b) proposed this shear zone is due to the collision of the Nico Pérez Terrane and the Río de La Plata Craton, suggesting

the onset of the deformation at 630–625 Ma, with dextral shearing up to 596 Ma and subsequent sinistral shearing at 594–584 Ma.

Another important shear zone occurring in the Nico Pérez Terrane is the Cueva del Tigre shear zone (Preciozzi *et al.*, 1979) developed at the boundary between the Valentines and Pavas blocks (Fig. 2). It is represented by a group of granitic mylonites, schists and phyllonites. This shear zone affected both, the Archean basement and the Neoproterozoic intrusions (Oriolo *et al.*, 2016b).

3. Previous radiometric data of the Nico Pérez Terrane

The available ages for the three structural blocks of Nico Pérez Terrane are displayed in the table 1. The pioneer works of Soliani (1986) and Cordani and Soliani (1990) reported Paleoproterozoic and Neoproterozoic ages for the Rivera Block. These

TABLE 1. GEOCHRONOLOGICAL AVAILABLE DATA FOR THE NICÓ PÉREZ TERRANE.

Unit	Age (Ma)	Method	Litology	Interpretation	Event Interpretation	Reference
La China Complex	2787±6	Zr: LA-ICP-MS: U-Pb	Deformed Granite	crystallization	Neoarchean Magmatism. Event 2.	Gaucher <i>et al.</i> (2014a)
La China Complex	3029±54	Zr: LA-ICP-MS: U-Pb	Biotitic Orthogneiss	crystallization	Mesoarchean Magmatism. Event 1.	Gaucher <i>et al.</i> (2010a)
La China Complex	3096±45	Zr: LA-ICP-MS: U-Pb	Metatonalite	crystallization	Mesoarchean Magmatism. Event 1.	Gaucher <i>et al.</i> (2011)
La China Complex	2690±42	Zr: LA-ICP-MS: U-Pb	Metatonalite	metamorphism	Neoarchean Metamorphism. Event 2.	Gaucher <i>et al.</i> (2011)
La China Complex	2718±8	Zr: LA-ICP-MS: U-Pb	Amphybolic Orthogneiss	crystallization	Neoarchean Magmatism. Event 2.	Gaucher <i>et al.</i> (2014a)
La China Complex	3408±16	Zr-SHRIMP U-Pb	Metatonalite	inheritance	Palaeoarchean basement inheritance	Hartmann <i>et al.</i> (2001)
La China Complex	3100±100	Zr-SHRIMP U-Pb	Metatonalite	crystallization	Mesoarchean Magmatism. Event 1.	Hartmann <i>et al.</i> (2001)
La China Complex	2721±7	Zr-SHRIMP U-Pb	Metatonalite	metamorphism	Neoarchean Metamorphism. Event 2.	Hartmann <i>et al.</i> (2001)
La China Complex	2707±6.9	Zr-SHRIMP U-Pb	Foliated Leucogranite	crystallization	Neoarchean Magmatism. Event 2.	This work
Las Tetas Complex	3222±5	Zr-SHRIMP U-Pb	Muscovitic Quartzite	source age	Palaeo to Mesorchean Source age.	Hartmann <i>et al.</i> (2001)
Las Tetas Complex	3263±14	Zr-SHRIMP U-Pb	Muscovitic Quartzite	source age	Palaeo to Mesorchean Source age.	Hartmann <i>et al.</i> (2001)
Las Tetas Complex	3181±6	Zr-SHRIMP U-Pb	Muscovitic Quartzite	source age	Palaeo to Mesorchean Source age.	Hartmann <i>et al.</i> (2001)
Las Tetas Complex	3146±4	Zr-SHRIMP U-Pb	Muscovitic Quartzite	source age	Palaeo to Mesorchean Source age.	Hartmann <i>et al.</i> (2001)
Valentines Formation	2968±12	Zr-SHRIMP U-Pb	Metaconglomerate	source age	Palaeo to Mesorchean Source age. Event 1.	Hartmann <i>et al.</i> (2001)
Valentines Formation	2762±8	Zr-SHRIMP U-Pb	Metaconglomerate	source age	Neoarchean Source age. Event 2.	Hartmann <i>et al.</i> (2001)
VRGC	2619±8	Zr-SHRIMP U-Pb	Granulite	inheritance	Neoarchean basement inheritance	Santos <i>et al.</i> (2003)
VRGC	2535±12	Zr-SHRIMP U-Pb	Granulite	inheritance	Neoarchean basement inheritance	Santos <i>et al.</i> (2003)
VRGC	2224±4	Zr-SHRIMP U-Pb	Granulite	inheritance	Transamazonic basement inheritance	Santos <i>et al.</i> (2003)

table 1 continued.

Unit	Age (Ma)	Method	Litology	Interpretation	Event Interpretation	Reference
VRGC	2163±8	Zr-SHRIMP U-Pb	Granulite	crystallization	Transamazonic Magmatism	Santos <i>et al.</i> (2003)
VRGC	2058±3	Zr-SHRIMP U-Pb	Granulite	metamorphism	Transamazonic Metamorphism	Santos <i>et al.</i> (2003)
VRGC	2106±21	Zr: LA-ICP-MS: U-Pb	Felsic Orthogneiss	crystallization	Transamazonic Magmatism	Oriolo <i>et al.</i> (2016a)
VRGC	<i>ca.</i> 2700	Zr: LA-ICP-MS: U-Pb	Felsic Orthogneiss	inheritance	Neoarchean basement inheritance	Oriolo <i>et al.</i> (2016a)
VRGC	2048±11	Zr: SHRIMP U-Pb	Mylonitized Granite	crystallization	Transamazonic Magmatism	Oriolo <i>et al.</i> (2016b)
VRGC	2163±8	Zr-SHRIMP U-Pb	Trondhjemite	inheritance	Transamazonic basement inheritance	Santos <i>et al.</i> (2003)
VRGC	2140±6	Zr-SHRIMP U-Pb	Trondhjemite	crystallization	Transamazonic Magmatism	Santos <i>et al.</i> (2003)
VRGC	2077±6	Zr-SHRIMP U-Pb	Trondhjemite	metamorphism	Transamazonic Metamorphism	Santos <i>et al.</i> (2003)
VRGC	2171.7±8.4	Zr-SHRIMP U-Pb	Leucocratic Gneiss	crystallization	Transamazonic Magmatism	Oyhantçabal <i>et al.</i> (2012)
VRGC	2139±73	Zr-SHRIMP U-Pb	Leucocratic Gneiss	metamorphism	Transamazonic Metamorphism	Oyhantçabal <i>et al.</i> (2012)
VRGC	587±19	Zr-SHRIMP U-Pb	Leucocratic Gneiss	metamorphism	Transamazonic Metamorphism	Oyhantçabal <i>et al.</i> (2012)
VRGC	1976±3	Mn-Th-U-Pb-EMP	Leucocratic Gneiss	metamorphism	Transamazonic Metamorphism	Oyhantçabal <i>et al.</i> (2012)
VRGC	2147±8.7	Zr-SHRIMP U-Pb	Mesocratic Gneiss	crystallization	Transamazonic Magmatism	Oyhantçabal <i>et al.</i> (2012)
VRGC	2113.7±3.1	Zr-SHRIMP U-Pb	Mesocratic Gneiss	crystallization	Transamazonic Magmatism	Oyhantçabal <i>et al.</i> (2012)
VRGC	1981±2	Mn-Th-U-Pb-EMP	Mesocratic Gneiss	metamorphism	Transamazonic Metamorphism	Oyhantçabal <i>et al.</i> (2012)
VRGC	2094±17	Zr-SHRIMP U-Pb	Mesocratic Gneiss	metamorphism	Transamazonic Metamorphism	Oyhantçabal <i>et al.</i> (2012)
VRGC	2095±15	Zr: LA-ICP-MS: U-Pb	Mafic Granulite	crystallization	Transamazonic Magmatism	Oriolo <i>et al.</i> (2016a)
VRGC	2041±24	Zr: LA-ICP-MS: U-Pb	Mafic Granulite	metamorphism	Transamazonic Metamorphism	Oriolo <i>et al.</i> (2016a)
VRGC	2069±16	Zr: LA-ICP-MS: U-Pb	Felsic Orthogneiss	metamorphism	Transamazonic Metamorphism	Oriolo <i>et al.</i> (2016a)
VRGC	2087±7.3	Zr: LA-ICP-MS: U-Pb	TG Gneiss	crystallization	Transamazonic Magmatism	Oriolo <i>et al.</i> (2016a)
VRGC	1857±45	Zr: LA-ICP-MS: U-Pb	TG Gneiss	metamorphism	?	Oriolo <i>et al.</i> (2016a)
VRGC	1790±50	Rb/Sr WR	Gneiss	?	?	Cordani and Soliani (1990)
VRGC	2140±150	Rb/Sr WR	Gneiss	metamorphism	Transamazonic metamorphism	Cordani and Soliani (1990)
VRGC	2030±70	Rb/Sr WR	Gneiss	metamorphism	Transamazonic metamorphism	Cordani and Soliani (1990)

table 1 continued.

Unit	Age (Ma)	Method	Litology	Interpretation	Event Interpretation	Reference
VRGC	2190±80	Rb/Sr WR	Gneiss	metamorphism	Transamazonic metamorphism	Cordani and Soliani (1990)
VRGC	2250±10	Rb/Sr WR	Gneiss	metamorphism	Transamazonic metamorphism	Cordani and Soliani (1990)
VRGC	2180±70	Rb/Sr WR	Gneiss	metamorphism	Transamazonic metamorphism	Cordani and Soliani (1990)
VRGC	946±31	K-Ar Kf	Gneiss	metamorphism	Tonian event?	Cordani and Soliani (1990)
VRGC	968±14	K-Ar Kf	Gneiss	metamorphism	Tonian event?	Cordani and Soliani (1990)
VRGC	2200±60	Rb/Sr WR	Gneiss	metamorphism	Transamazonic metamorphism	Cordani and Soliani (1990)
VRGC	2220±90	Rb/Sr WR	Gneiss	metamorphism	Transamazonic metamorphism	Cordani and Soliani (1990)
VRGC	2240±110	Rb/Sr WR	Gneiss	metamorphism	Transamazonic metamorphism	Cordani and Soliani (1990)
VRGC	560±70	Rb/Sr WR	Metatonalite	magmatism	Brasiliano Magmatism	Cordani and Soliani (1990)
VRGC	540±90	Rb/Sr WR	Tonalite	magmatism	Brasiliano Magmatism	Cordani and Soliani (1990)
Undifferentiated granites (RB)	507±12	K-Ar Pg	Tonalite	magmatism	Brasiliano Magmatism	Cordani and Soliani (1990)
Undifferentiated granites (RB)	586±22	K-Ar Hbl	Tonalite	magmatism	Brasiliano Magmatism	Cordani and Soliani (1990)
Undifferentiated granites (RB)	536±11	K-Ar WR	Microgranite	magmatism	Brasiliano Magmatism	Cordani and Soliani (1990)
Undifferentiated granites (RB)	584±15	K-Ar Pg	Granodiorite	magmatism	Brasiliano Magmatism	Cordani and Soliani (1990)
Undifferentiated granites (RB)	589±8	K-Ar Bt	Granodiorite	magmatism	Brasiliano Magmatism	Cordani and Soliani (1990)
Undifferentiated granites (RB)	576±10	K-Ar Bt	Granodiorite	magmatism	Brasiliano Magmatism	Cordani and Soliani (1990)
Undifferentiated granites (RB)	499±12	K-Ar Pg	Granodiorite	magmatism	Brasiliano Magmatism	Cordani and Soliani (1990)
Undifferentiated granites (RB)	523±13	K-Ar WR	Microgranite	magmatism	Brasiliano Magmatism	Cordani and Soliani (1990)
Undifferentiated granites (RB)	540±90	Rb/Sr WR	Granite	magmatism	Brasiliano Magmatism	Cordani and Soliani (1990)
Undifferentiated granites (RB)	515±11	K-Ar Bt	Granite	magmatism	Brasiliano Magmatism	Cordani and Soliani (1990)
Undifferentiated granites (RB)	537±15	K-Ar WR	Microgranite	magmatism	Brasiliano Magmatism	Cordani and Soliani (1990)
Sobresaliente Granite	2043±44	Zr-SHRIMP U-Pb	Quartz Monzonite	crystallization	Brasiliano Magmatism	Oyhantçabal <i>et al.</i> (2012)
Sobresaliente Granite	578.1±5.8	Zr-SHRIMP U-Pb	Quartz Monzonite	crystallization	Brasiliano Magmatism	Oyhantçabal <i>et al.</i> (2012)
Las Flores Granite	586±2.7	Zr-SHRIMP U-Pb	Granite	crystallization	Brasiliano Magmatism	Oyhantçabal <i>et al.</i> (2012)
Las Flores Granite	578±10	K -Ar Bt	Granite	crystallization	Brasiliano Magmatism	Oyhantçabal <i>et al.</i> (2012)
Las Flores Granite	579±20	K-Ar Bt	Granodiorite	magmatism	Brasiliano Magmatism	Cordani and Soliani (1990)

table 1 continued.

Unit	Age (Ma)	Method	Litology	Interpretation	Event Interpretation	Reference
Las Flores Granite	370±7	K-Ar Bt	Granodiorite	magmatism	Brasiliano Magmatism	Cordani and Soliani (1990)
Las Flores Granite	1200±? (sic)	Rb/Sr WR	Granodiorite	magmatism	Brasiliano Magmatism	Cordani and Soliani (1990)
Amarillo granite	2530±26	Zr: LA-ICP-MS: U-Pb	Leucogranite	inheritance	Archean inheritance	Oriolo <i>et al.</i> (2016a)
Amarillo Granite	596±2.3	Zr: LA-ICP-MS: U-Pb	Leucogranite	crystallization	Brasiliano Magmatism	Oriolo <i>et al.</i> (2016a)
Illescas Granite	1760±30	Rb/Sr	Rapakivi Granite	crystallization	Statherian Extensional Magmatism	Bossi and Campal (1992)
Illescas Granite	1784±5	Pb-Pb	Rapakivi Granite	crystallization	Statherian Extensional Magmatism	Campal and Schipilov (1995)
Illescas Granite	1734±11	Zr-SHRIMP U-Pb	Rapakivi Granite	crystallization	Statherian Extensional Magmatism	This work
Illescas Granite	1768±11	U-Pb LA-ICP-MS	Rapakivi Granite	crystallization	Statherian Extensional Magmatism	Oriolo <i>et al.</i> (2019)
Zapican Diorite	610.4±2.5	Zr: LA-ICP-MS: U-Pb	Tonalite-Granodiorite	crystallization	Brasiliano Magmatism	Oriolo <i>et al.</i> (2016a)
Zapican Diorite	3045±26	Zr: LA-ICP-MS: U-Pb	Tonalite-Granodiorite	inheritance	Archean inheritance	Oriolo <i>et al.</i> (2016a)
Zapican Diorite	585.8±5.7	Zr-SHRIMP U-Pb	Tonalitic Gneiss	crystallization	Brasiliano Magmatism	This work
Cerro de las Cuentas Granite	2118±62	Zr-SHRIMP U-Pb	Deformed Granite	inheritance	Transamazonic basement inheritance	This work
Cerro de las Cuentas Granite	584.4±8.2	Zr-SHRIMP U-Pb	Deformed Granite	crystallization	Brasiliano Magmatism	This work
Cerro Chato Granite	~2190	Zr-SHRIMP U-Pb	Granite	inheritance	Transamazonic basement inheritance	This work
Cerro Chato Granite	~1492	Zr-SHRIMP U-Pb	Granite	inheritance	Mesoproterozoic basement inheritance	This work
Cerro Chato Granite	639±98	Zr-SHRIMP U-Pb	Granite	crystallization	Brasiliano Magmatism	This work
Cueva del Tigre shear zone	3087±13	Zr-SHRIMP U-Pb	Mylonitized Granite	inheritance	Mesoarchean basement inheritance	This work
Cueva del Tigre shear zone	588.0±6.1	Zr-SHRIMP U-Pb	Mylonitized Granite	crystallization	Brasiliano Magmatism	This work
Cueva del Tigre shear zone	3089±11	Zr-SHRIMP U-Pb	Mylonitized Granite	crystallization	Mesorchean Magmatism. Event 1.	This work
Cueva del Tigre shear zone	3092±5	Zr-SHRIMP U-Pb	Granitic Mylonite	crystallization	Mesorchean Magmatism. Event 1.	This work
Cueva del Tigre shear zone	~2142	Zr-SHRIMP U-Pb	Granitic Mylonite	metamorphism	Transamazonic Metamorphism	This work

table 1 continued.

Unit	Age (Ma)	Method	Litology	Interpretation	Event Interpretation	Reference
Rivera shear zone	1935±9	Mn-Th-U-Pb-EMP	Mylonite	?	-	Oyhantçabal <i>et al.</i> (2012)
Rivera shear zone	606±10	Mn-Th-U-Pb-EMP	Mylonite	shear	-	Oyhantçabal <i>et al.</i> (2012)
Rivera shear zone	510±18	Mn-Th-U-Pb-EMP	Mylonite	shear	-	Oyhantçabal <i>et al.</i> (2012)
Rivera shear zone	606±10.1	K-Ar Ms	Mylonite	shear	-	Oyhantçabal <i>et al.</i> (2012)
Rivera shear zone	366±31	K-Ar Bt	Cataclastic Granite	deformation	Ar lost	Cordani and Soliani (1990)
Rivera shear zone	414±29	K-Ar Bt	Cataclastic Granite	deformation	Ar lost	Cordani and Soliani (1990)
Rivera shear zone	569±4	Rb/Sr WR	Granite	magmatism	Brasiliano Magmatism	Cordani and Soliani (1990)
Rivera shear zone	569±4	Rb/Sr WR	Microgranite	magmatism	Brasiliano Magmatism	Cordani and Soliani (1990)
Rivera shear zone	569±4	Rb/Sr WR	Granite	magmatism	Brasiliano Magmatism	Cordani and Soliani (1990)
Sarandí del Yi shear zone	2025±37	Zr: LA-ICP-MS: U-Pb	Mylonite	crystallization	Transamazonic Magmatism	Oriolo <i>et al.</i> (2016b)
Sarandí del Yi shear zone	623±5	Zr: LA-ICP-MS: U-Pb	Mylonite	dynamo-metamorphism	Brasiliano deformation	Oriolo <i>et al.</i> (2016b)
Sarandí del Yi shear zone	590.2±2.8	Ar/Ar hbl	Mylonite	dynamo-metamorphism	Brasiliano deformation	Oriolo <i>et al.</i> (2016b)
Sarandí del Yi shear zone	2048±11	Zr: LA-ICP-MS: U-Pb	Granitic Mylonite	crystallization	Transamazonic Magmatism	Oriolo <i>et al.</i> (2016b)
Sarandí del Yi shear zone	2115±38	Zr: LA-ICP-MS: U-Pb	Deformed Granitoid	crystallization	Transamazonic Magmatism	Oriolo <i>et al.</i> (2016b)
Sarandí del Yi shear zone	589.1±1.6	Zr: LA-ICP-MS: U-Pb	Deformed Granitoid	dynamo-metamorphism	Brasiliano deformation	Oriolo <i>et al.</i> (2016b)
Sarandí del Yi shear zone	2068.9±4.2	Zr: LA-ICP-MS: U-Pb	Ultramylonite	dynamo-metamorphism	Transamazonic Deformation	Oriolo <i>et al.</i> (2016b)
Sarandí del Yi shear zone	596.0±3.3	Zr: LA-ICP-MS: U-Pb	Mylonite	crystallization	Brasiliano Magmatism	Oriolo <i>et al.</i> (2016b)
Sarandí del Yi shear zone	600.1±3.4	Ar/Ar Ms	Mylonite	?	?	Oriolo <i>et al.</i> (2016b)
Sarandí del Yi shear zone	566±2.9	Rb/Sr WR	Mylonite	dynamo-metamorphism	Brasiliano deformation	Oriolo <i>et al.</i> (2016b)
Sarandí del Yi shear zone	594.41±0.99	Ar/Ar Ms	Mylonite	dynamo-metamorphism	Brasiliano deformation	Oriolo <i>et al.</i> (2016b)

authors obtained a Rb-Sr (WR) isochron of 2250 ± 60 Ma for the quartz-feldspathic gneissic basement; also, Cordani and Soliani (1990) obtained several K-Ar ages in biotite, plagioclase, and whole rock around 500-600 Ma. Recently, Santos *et al.* (2003), Oyhantçabal *et al.* (2012) and Oriolo *et al.* (2016a) obtained several U-Pb single crystal zircon ages within the interval 2200-2000 Ma, for the high grade gneisses, which

were interpreted as crystallization ages of the magmatic protoliths, confirming the paleoproterozoic age of the block. Oriolo *et al.* (2016a) and Oyhantçabal *et al.* (2012) also reported a few ages around 580 Ma for Ediacaran granitic plutons.

In Valentines Block only a few U-Pb zircon ages have been obtained. Hartmann *et al.* (2001) reported Archean detrital zircon ages between 3000 and

2700 Ma in a metaconglomerate (Valentines BIF's). For metagranites of this unit Santos *et al.* (2003), obtained ages between 2619 and 2058 Ma. More recently, Oriolo *et al.* (2016b) obtained two Paleoproterozoic ages for Valentines-Rivera Granulitic Complex of 2016 and 2048 Ma.

The Pavas Block also has a few geochronological data available. As mentioned above, Hartmann *et al.* (2001) obtained U-Pb zircon SHRIMP ages of 3400 Ma for zircon cores and 2700 Ma for zircon rims in a tonalitic orthogneiss of the La China Complex. Gaucher *et al.* (2011, 2014b) obtained a zircon U-Pb LA-ICP-MS age of 3096 Ma for the same lithology, and detrital zircon ages of 3000, 2970, 2760 and 2600 Ma in a metaconglomerate of the Las Tetas Complex.

All the magmatic crystallization ages (*e.g.*, zircon nuclei with Th/U ratios greater than 0.1) reported by the different authors (Hartmann *et al.*, 2001; Gaucher *et al.*, 2011, 2014a and references therein) for the metatonalites from La China Complex can be grouped into Mesoarchean (3.03 Ga) and Neoarchean (2.79–2.72 Ga). On the other hand, metamorphic events (*e.g.*, zircon rims with Th/U ratios less than 0.1) show Mesoarchean (3.1 Ga) and Neoarchean (2.69 Ga) ages. Detrital zircons found in the Las Tetas Complex suggest Archean source areas and a maximum Mesoarchean deposition age (Loureiro *et al.*, 2019 and references therein).

The intrusive Illescas granite was dated by Bossi and Campal (1992) by whole-rock Rb-Sr method, yielding 1760 ± 32 Ma; later Campal and Schipilov (1995) reported a Pb-Pb age of 1784 ± 5 Ma. More recently Oriolo *et al.* (2019) obtained a zircon U-Pb LA-ICP-MS age of 1768 ± 11 Ma for this granite.

Younger ages reported in the Nico Pérez Terrane are 739 ± 20 Ma (Rb-Sr WR) for the Cerro Chato granite (Bossi and Campal, 1987), and 610 Ma for the Zapicán diorite that intrudes La China Complex (Oriolo *et al.*, 2016a).

4. Results of U-Pb zircon geochronology

New U-Pb SHRIMP zircon results on eight samples of granitoid rocks are presented in this work with the goal of constraining the tectonic evolution of the Nico Pérez Terrane. The analytical data are included in table 2. The zircon crystals were extracted from the samples by conventional methods, mounted in epoxy mounts, together with

a few fragments of the TEMORA-2 standard, and polished. Then, cathodoluminescence images were obtained to reveal their internal structure to target the best sites for the U-Pb isotopic analyses. All measurements were made at Centro de Pesquisas Geocronológicas (CPGeo) of the University of São Paulo (USP), Brazil.

The eight samples were taken from six outcrops and were analyzed using the SHRIMP-II instrument of the CPGeo. Details of the analytical procedures, including the calibration methods, were presented by Williams (1998) and the work at the São Paulo laboratory was described by Sato *et al.* (2014). U abundance and U/Pb values of the studied zircon crystals were calibrated against the Z6266 (903 ppm) and the TEMORA-2 (416.78 Ma) standards, respectively. Individual ages were determined from five successive scans of the mass spectrum, and the ages reported in the text are with 95% confidence limits. Correction for common Pb was made using the measured ^{204}Pb , and the typical error component for the $^{206}\text{Pb}/^{238}\text{U}$ ratios is less than 2 percent. The data were reduced by using a SQUID software and the Concordia diagrams were prepared using Isoplot /Ex (Ludwig, 2009).

Zircons are typically prismatic to equant, where several present oscillatory zoning. Some crystals present homogeneous cores, either bright or dark. In many cases the crystals are fragmented. The cathodoluminescence images of representative analyzed zircons are shown in figure 5. The concordia diagrams for each analyzed sample are shown in figures 6 to 13.

4.1. Sample NP-07-Cerro de las Cuentas foliated granitoid

This sample was collected at Cerro de las Cuentas granite, in the northernmost part of the Valentines Block (Fig. 2). This granite intrudes the Valentines-Rivera Granulitic Complex, and it corresponds to an equigranular fine-grained foliated granite, composed of quartz+K-feldspar+plagioclase+biotite. The deformation is not observed in the outcrop scale, but undulose extinction and bulging recrystallization in quartz crystals occur. Zircon crystals are mostly prismatic showing oscillatory zoning and some recrystallization phenomena (Fig. 5b). A total of nine spots out of six zircon crystals were analyzed (Table 2). Three zircon grains (#1, #2 and #7) were

TABLE 2. U-PB SHRIMP ANALYTICAL DATA.

Spot Name	Ratios				7-corr % Com		Age (Ma)			Disc %	ppm	Th/U				
	$^{207}\text{Pb}/^{235}\text{U}$	err %	$^{206}\text{Pb}/^{238}\text{U}$	err %	$^{207}\text{Pb}/^{206}\text{Pb}$	err %	Corr	^{206}Pb	$^{206}\text{Pb}/^{238}\text{U}$							
NP-02																
NP-02-1.1	4.538	9.4	0.3078	2.6	0.1069	9.1	0.277	5.1	1730	40	1748	166	1	17	31	1.89
NP-02-2.1	4.2972	5.8	0.3034	2.1	0.1027	5.4	0.365	2.43	1708	32	1674	100	-2	24	44	1.91
NP-02-3.1	4.6821	5.8	0.3144	2.3	0.108	5.3	0.399	2.51	1762	36	1766	97	0	18	36	2.07
NP-02-4.1	4.6442	4.8	0.3109	2	0.1084	4.4	0.408	2.69	1745	30	1772	80	2	27	64	2.41
NP-02-5.1	3.9035	8.8	0.2807	3.8	0.1009	8	0.432	5.38	1595	54	1640	148	3	31	92	3.04
NP-02-6.1	4.6946	6.2	0.3002	3.5	0.1134	5.1	0.561	2.98	1692	52	1855	93	10	25	48	2
NP-02-7.1	4.4173	2.1	0.3036	1.9	0.1055	0.8	0.929	0.39	1709	29	1723	14	1	209	265	1.31
NP-02-8.1	4.4764	2	0.2972	1.8	0.1092	0.9	0.893	1.11	1677	27	1787	17	7	147	182	1.28
NP-02-9.1	4.4883	2	0.3069	1.8	0.1061	0.8	0.918	0.4	1725	27	1733	14	1	213	429	2.08
NP-02-10.1	4.5553	2.1	0.3109	1.3	0.1063	1.7	0.585	0.83	1745	19	1736	32	-1	77	110	1.47
NP-02-11.1	4.2422	60.3	0.2739	6.9	0.1123	60	0.114	31.19	1560	95	1838	1086	17	101	235	2.4
NP-02-12.1	4.5677	2.1	0.3118	2	0.1063	0.7	0.952	0.01	1749	31	1736	12	-1	213	207	1.01
NP-07																
NP-07-1.1	0.8114	2.8	0.0957	1	0.0615	2.6	0.35	0.89	589	5	657	56	11	277	184	0.69
NP-07-1.2	0.7253	9.6	0.0906	2.5	0.0581	9.3	0.262	3.45	559	13	533	203	-5	142	159	1.15
NP-07-2.1	0.7161	2.7	0.0864	1.7	0.0601	2.1	0.637	1.07	534	9	608	45	13	1,086	354	0.34
NP-07-2.2	0.7748	2.2	0.0941	1.6	0.0597	1.6	0.693	0.6	580	9	593	35	2	606	449	0.77
NP-07-3.1	0.7844	5.8	0.0956	2.1	0.0595	5.5	0.361	1.82	588	12	586	118	0	164	280	1.76
NP-07-5.1	0.6915	8.1	0.0809	1.1	0.062	8.1	0.138	7.49	501	5	675	172	27	376	208	0.57
NP-07-6.1	0.7029	8.1	0.0826	1	0.0617	8.1	0.128	3.37	511	5	665	173	24	303	282	0.96
NP-07-7.1	5.5263	7.5	0.3165	4.9	0.1266	5.7	0.649	3.06	1773	76	2052	101	16	61	17	0.29
NP-07-7.2	4.1521	4.7	0.2505	2.8	0.1202	3.7	0.611	4.64	1441	37	1959	66	29	148	27	0.19

table 2 continued.

Spot Name	Ratios			7-eorr % Com			Age (Ma)			ppm			Th/U			
	$^{207}\text{Pb}/^{235}\text{U}$	err %	$^{206}\text{Pb}/^{238}\text{U}$	err %	$^{207}\text{Pb}/^{206}\text{Pb}$	err %	Corr	^{206}Pb	$^{206}\text{Pb}/^{238}\text{U}$	1σ	$^{207}\text{Pb}/^{206}\text{Pb}$	1σ	U	Th		
NP-08																
NP-08-1.1	0.3799	18.3	0.0477	1.9	0.0578	18.2	0.102	0.99	300	5	522	399	44	840	801	0.99
NP-08-2.1	0.7895	4.4	0.0959	1.2	0.0597	4.3	0.262	1.19	591	7	592	93	0	346	399	1.19
NP-08-2.2	0.7909	4.3	0.0939	1.4	0.0611	4.1	0.319	1.08	578	8	643	87	11	334	349	1.08
NP-08-3.1	0.757	4.8	0.0831	1.2	0.0661	4.7	0.24	0.93	514	6	810	98	38	325	291	0.93
NP-08-3.2	0.747	6.6	0.0788	1.5	0.0687	6.4	0.228	0.78	489	7	891	132	47	472	356	0.78
NP-08-4.1	0.6809	14.3	0.0848	1.9	0.0582	14.2	0.133	5.05	525	10	538	310	2	284	1387	5.05
NP-08-5.1	0.5775	23.7	0.0549	6.4	0.0763	22.8	0.27	1.11	345	21	1102	456	71	610	657	1.11
NP-08-6.1	3.3441	12.8	0.2602	3	0.0932	12.4	0.234	1.61	1491	40	1492	235	0	12	19	1.61
NP-08-7.1	7.7668	1.1	0.4096	1	0.1375	0.5	0.895	0.57	2213	19	2196	9	-1	278	153	0.57
NP-08-7.2	7.3953	2.3	0.3929	1.8	0.1365	1.4	0.8	0.44	2136	33	2183	24	3	357	153	0.44
NP-09A																
NPP9A-1.1	0.814	2.4	0.0985	2.2	0.0599	0.9	0.921	0.07	606	13	600	20	-1	764	310	0.42
NPP9A-10.1	0.791	2.2	0.095	1.8	0.0604	1.2	0.823	0.3	585	10	618	27	6	648	825	1.32
NPP9A-10.2	0.8124	3.1	0.0968	1.8	0.0609	2.5	0.579	0.45	596	10	634	54	6	215	110	0.53
NPP9A-11.1	0.7565	3.5	0.0915	2.7	0.0599	2.2	0.764	0.43	565	14	601	49	6	279	135	0.5
NPP9A-12.1	0.8054	3.6	0.0971	2.3	0.0601	2.8	0.634	0.3	597	13	609	60	2	151	117	0.8
NPP9A-2.1	19.5413	2.2	0.6011	2.2	0.2358	0.4	0.987	1.61	3034	52	3092	6	2	231	90	0.4
NPP9A-2.2	0.7426	2.5	0.0915	2	0.0588	1.6	0.786	0.31	565	11	561	34	-1	661	317	0.5
NPP9A-2.3	19.799	1.8	0.6143	1.8	0.2337	0.4	0.977	-0.25	3087	44	3078	6	0	186	102	0.57
NPP9A-3.1	0.8051	2.5	0.0968	1.7	0.0603	1.8	0.685	0.37	596	10	614	39	3	382	208	0.56
NPP9A-4.1	0.7493	3.8	0.0904	2.2	0.0601	3.1	0.585	1.28	558	12	607	67	8	389	183	0.49
NPP9A-4.2	0.8079	1.7	0.0978	1.6	0.0599	0.5	0.948	0.05	601	9	601	12	0	2129	845	0.41
NPP9A-5.1	0.8003	2.2	0.0945	1.8	0.0614	1.2	0.839	0.35	582	10	653	26	11	540	234	0.45
NPP9A-6.1	0.7806	11.6	0.0911	2.6	0.0622	11.3	0.227	3.54	562	14	680	242	18	108	75	0.72

table 2 continued.

Spot Name	Ratios				err	7-corr % Corr	Age (Ma)			Disc %	ppm	Th/U
	$^{207}\text{Pb}/^{235}\text{U}$	err %	$^{206}\text{Pb}/^{238}\text{U}$	err %	$^{207}\text{Pb}/^{206}\text{Pb}$	err %	$^{206}\text{Pb}/^{238}\text{U}$	1σ	$^{207}\text{Pb}/^{206}\text{Pb}$	1σ	U	Th
NP09A-7.1	0.7497	2.6	0.0889	1.9	0.0611	1.8	0.737	0.56	549	10	644	38
NP09A-8.1	0.8501	3.4	0.0952	2.1	0.0647	2.6	0.623	1.63	586	12	766	56
NP09A-9.1	0.8095	3.9	0.0948	1.8	0.0619	3.4	0.476	0.79	584	10	672	73
NP09A-9.2	0.7719	3.5	0.0936	1.8	0.0598	3.1	0.495	0.74	577	10	597	67
NP-09B1												
NP-09B1-1.1	17.5302	2.5	0.5566	2.5	0.2284	0.4	0.989	4.21	2852	57	3041	6
NP-09B1-1.2	20.0772	1.9	0.6137	1.9	0.2373	0.5	0.97	0.52	3085	45	3102	7
NP-09B1-2.1	20.1609	1.8	0.6116	1.7	0.2374	0.3	0.981	0.29	3094	43	3102	5
NP-09B1-3.1	20.3395	2.4	0.6207	2.2	0.2377	0.9	0.929	-0.18	3113	54	3104	14
NP-09B1-4.1	19.2974	1.8	0.5928	1.8	0.2361	0.4	0.973	2.53	3001	43	3094	7
NP-09B1-4.2	15.6391	2.7	0.5239	2.5	0.2165	1	0.929	4.64	2716	56	2955	16
NP-09B1-5.1	19.6023	1.8	0.6077	1.8	0.2339	0.4	0.974	0.63	3061	44	3079	7
NP-09B1-6.1	19.6229	1.8	0.6065	1.8	0.2347	0.4	0.98	0.83	3056	43	3084	6
NP-09B1-7.1	18.8948	2.4	0.5864	2.4	0.2337	0.5	0.978	2.69	2975	56	3077	8
NP-09B1-8.1	18.5771	2.8	0.5811	2.7	0.2319	0.5	0.982	2.94	2953	65	3065	8
NP-09B2												
NP-09B2-1.1	19.3056	2.2	0.5851	2.1	0.2393	0.7	0.946	3.83	2970	50	3115	11
NP-09B2-2.1	6.4596	2	0.368	1.8	0.1273	0.8	0.923	0.47	2020	32	2061	14
NP-09B2-3.1	17.8835	2.4	0.5716	2.4	0.2269	0.3	0.99	2.71	2914	56	3030	6
NP-09B2-4.1	19.4037	1.9	0.5978	1.8	0.2354	0.5	0.971	1.9	3021	44	3089	7
NP-09B2-5.1	19.674	2.1	0.6049	2	0.2359	0.6	0.953	1.39	3049	49	3093	10
NP-09B2-6.1	19.926	1.9	0.61	1.9	0.2369	0.5	0.963	0.9	3070	46	3099	8
NP-09B2-7.1	19.5011	3	0.6	2.9	0.2357	0.8	0.961	1.75	3030	70	3091	13
NP-09B2-8.1	19.4858	2.7	0.5967	2.6	0.2368	0.6	0.976	2.26	3017	62	3099	9
NP-09B2-9.1	12.0421	2.7	0.4563	1.9	0.1914	2	0.677	5.04	2423	38	2754	33

table 2 continued.

Spot Name	Ratios				7-corr % Com		Age (Ma)			ppm		Th/U				
	$^{207}\text{Pb}/^{235}\text{U}$	err %	$^{206}\text{Pb}/^{238}\text{U}$	err %	$^{207}\text{Pb}/^{206}\text{Pb}$	err %	Corr	$^{206}\text{Pb}/^{238}\text{U}$	1σ	$^{207}\text{Pb}/^{206}\text{Pb}$	1σ	Disc %	U	Th		
NP-09B2-9.2	18.7904	2.5	0.5791	2.4	0.2353	0.8	0.951	3.57	2945	57	3089	13	6	294	98	0.35
NP-09B2-10.1	20.02	2	0.6153	2	0.236	0.3	0.988	0.12	3091	48	3093	5	0	274	185	0.7
NP-09B2-10.2	7.1207	2.6	0.3496	1.8	0.1477	1.9	0.699	3.87	1933	31	2320	32	19	380	30	0.08
NP-09B2-11.1	19.0146	2.3	0.5879	2.3	0.2346	0.4	0.987	2.58	2981	54	3084	6	4	212	104	0.51
NP-09B2-11.2	19.1292	1.9	0.5892	1.8	0.2355	0.4	0.972	2.75	2986	43	3090	7	4	167	70	0.43
NP-09B2-12.1	18.8599	2.5	0.5853	1.9	0.2337	1.7	0.745	2.85	2970	45	3078	27	4	136	73	0.56
NP-09B2-12.2	5.6148	2.4	0.3231	2.1	0.126	1.3	0.856	3.14	1805	33	2043	22	13	357	17	0.05
NP-10																
NP-10-1.1	0.5693	7.3	0.0738	2.7	0.056	6.8	0.374	5.4	459	12	451	150	-2	360	483	1.39
NP-10-2.1	0.8466	15.7	0.0942	1.8	0.0652	15.6	0.1112	9.18	580	10	780	329	27	87	85	1.01
NP-10-3.1	0.8276	3.6	0.0994	2	0.0604	3	0.564	0.3	611	12	617	64	1	163	213	1.35
NP-10-4.1	0.8489	4.6	0.0965	1.1	0.0638	4.5	0.249	1.88	594	7	735	95	20	142	194	1.41
NP-10-5.1	0.8249	2.9	0.0939	1.1	0.0637	2.6	0.388	1.06	579	6	732	56	22	158	216	1.41
NP-10-6.1	0.7753	3.4	0.094	1.7	0.0598	2.9	0.507	0.99	579	10	596	64	3	250	221	0.91
NP-10-7.1	0.8324	9.1	0.081	2.7	0.0745	8.7	0.299	5.41	502	13	1056	175	54	69	47	0.71
NP-10-8.1	0.7935	4.8	0.0944	2.6	0.061	4.1	0.531	1.33	581	14	639	88	9	133	116	0.9
NP-10-9.1	0.8076	3.6	0.0975	2.2	0.0601	2.8	0.607	0.69	600	12	606	61	1	261	407	1.61
NP-10-9.2	0.7691	6.7	0.0941	2.1	0.0593	6.3	0.309	2.2	580	11	577	138	0	113	112	1.02
NP-10-10.1	0.7687	4.2	0.0937	1.1	0.0595	4.1	0.271	0.86	577	6	586	89	2	116	100	0.89
NP-10-11.1	0.7866	5.4	0.0954	1.8	0.0598	5.1	0.329	1.24	587	10	596	110	2	96	103	1.1
NP-11																
NP-11-1.1	13.0171	2	0.5103	1.9	0.185	0.5	0.969	0.95	2658	42	2698	8	2	167	73	0.45
NP-11-2.1	13.3526	1.8	0.5249	1.7	0.1845	0.5	0.963	-0.24	2720	39	2694	8	-1	145	81	0.58
NP-11-2.2	12.9291	2.2	0.5087	1.5	0.1843	1.7	0.646	3.38	2651	32	2692	28	2	164	85	0.54
NP-11-3.1	13.1303	1.4	0.5109	1.2	0.1864	0.7	0.867	1.28	2660	27	2711	12	2	88	32	0.38
NP-11-4.1	13.6968	1.8	0.5345	1.8	0.1858	0.3	0.982	-0.9	2761	40	2706	6	-2	249	103	0.43

Spot Name	Ratios			Age (Ma)			Disc %	ppm	Th/U	
	$^{207}\text{Pb}/^{235}\text{U}$	err %	$^{206}\text{Pb}/^{238}\text{U}$	err %	$^{207}\text{Pb}/^{206}\text{Pb}$	err %	$^{206}\text{Pb}/^{238}\text{U}$	1σ	$^{207}\text{Pb}/^{206}\text{Pb}$	1σ
NP-11-5.1	11.9664	2	0.4667	1.7	0.186	1.1	0.838	5.3	2469	35
NP-11-6.1	13.7759	1.7	0.5382	1.6	0.1857	0.5	0.952	-1.17	2776	36
NP-11-7.1	13.6145	1.9	0.5315	1.8	0.1858	0.5	0.964	-0.61	2748	40
NP-11-8.1	13.3209	1.6	0.5151	1.6	0.1876	0.4	0.969	0.9	2678	34
NP-11-9.1	13.9916	1.5	0.544	1.5	0.1865	0.4	0.972	-1.62	2800	33
NP-11-10.1	13.5893	1.7	0.5317	1.6	0.1854	0.6	0.934	-0.81	2748	35
NP-11-11.1	13.9022	1.8	0.5428	1.7	0.1858	0.4	0.979	-1.66	2795	40

table 2 continued.

analyzed in their core and rim (Fig. 5b). Both, core and rim, yielded similar ages. Figure 6 shows the concordant age of 584±8 Ma obtained from three out of the six grains (highly discordant data was discarded). Based on zircon morphology and Th/U ratios (>0.34), this result is considered a good estimate for its crystallization age. Zircon #7 is an inherited xenocrystal, with a rather imprecise Rhyacian age of about 2100 Ma.

4.2. Sample NP-08-Cerro Chato granite

This sample was collected at the western margin of the Cerro Chato granite, in the central part of the Nico Pérez Terrane; also, it intrudes the Valentines-Rivera Granulitic Complex (Fig. 2). It is a fine to coarse-grained granite, sometimes porphyric, with large zoned feldspars, plagioclase, quartz, muscovite and biotite. Zircon, apatite, and epidote are also present as accessory minerals. Locally, this granite presents mylonitic foliation.

A total of ten spots were analysed out of seven zircon crystals (Table 2 and Fig. 5c). Zircon grains are prismatic, rounded, or fragmented, and show cores that are either light or dark homogeneous or zoned. Homogeneous dark rims are observed. Most of the analytical results show high discordance, and Pb loss is observed (Fig. 7). A concordant age of 591±7 Ma is obtained using two zircon grains (highly discordant data was discarded), probably it represents the crystallization age of this pluton. Two inherited crystals yielded Paleoproterozoic (*ca.* 2.1 Ga) and Mesoproterozoic (*ca.* 1.5 Ga) ages, respectively.

4.3. Samples NP-09A, NP-09B1 and NP-09B2-Mylonitic granites within the Cueva del Tigre shear zone

These samples were taken at an outcrop located within the Cueva de la Tigre shear zone in the contact of two deformed granitoids, affected by the shear zone (Fig. 2). Sample NP-09A is a granitoid specimen, classified in the field as protomylonitic granite, presenting quartz ribbons and quartz crystals with subgrain rotation and bulging recrystallization. Sample NP-09B is a foliated granitoid, showing a banded fabric, splitted into a lighter specimen (NP-09B1) and a darker one (NP-09B2) with some more biotite and less plagioclase due to mineral segregation. Petrographically, it is composed of

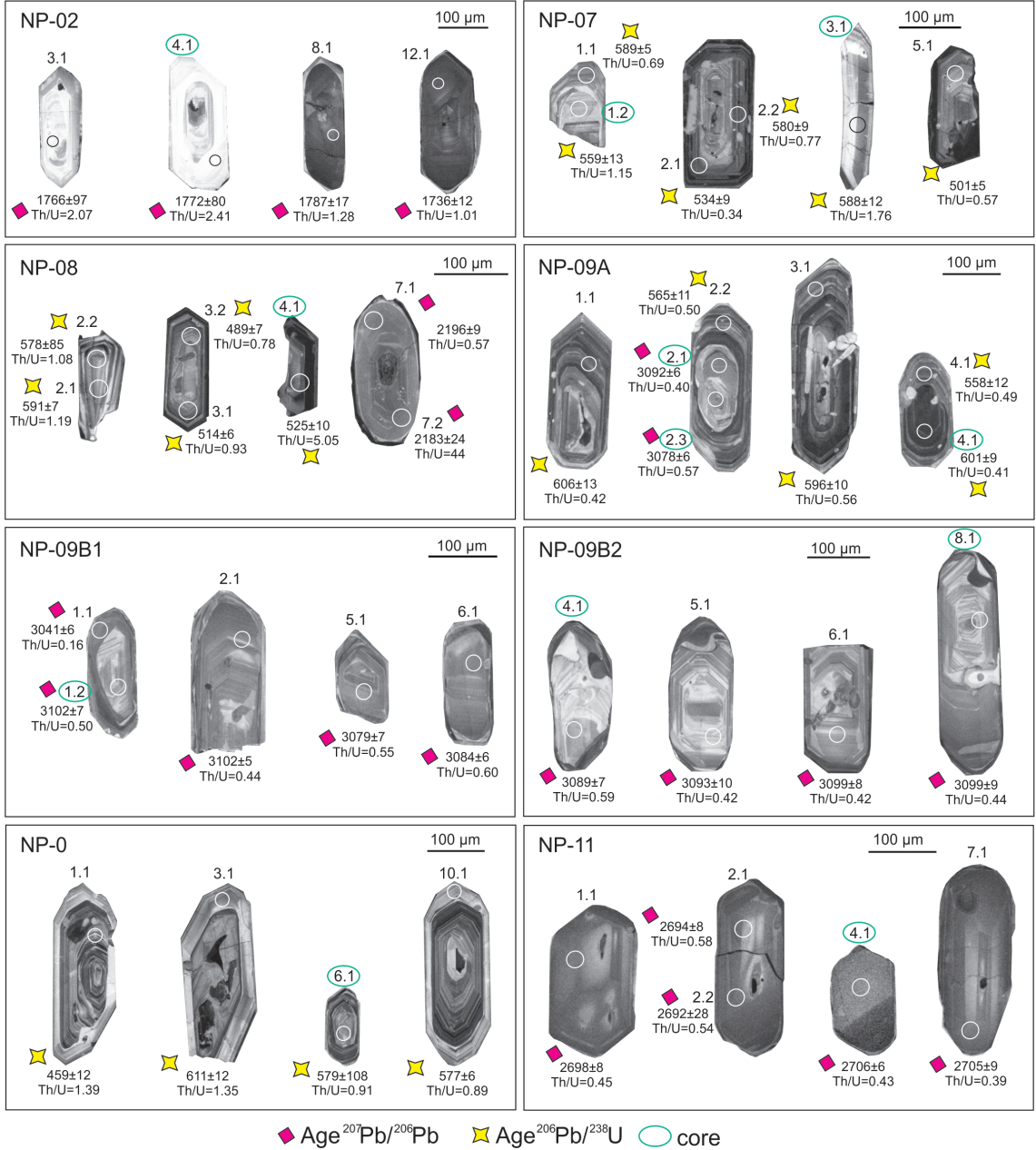


FIG. 5. The cathodoluminescence images of representative analyzed zircons.

quartz+K-feldspar+plagioclase+biotite and chlorite. K-feldspar crystals also show bulging recrystallization and undulose extinction.

Zircon grains in sample NP-09A are prismatic with oscillatory zoning, and some of them show xenocrystal cores. Twelve zircon crystals were analyzed in 17 spots. Figure 10 shows a concordant

age of 588.0 ± 6.1 Ma obtained from 10 spots out of 17 (discordant data was discarded), interpreted as the crystallization age. Xenocrystal core yielded Mesoarchean ages (#2.1 and #2.3 in Table 2). Besides, all the analyzed crystals of this sample exhibited Th/U ratios (0.40 to 1.32) typical of magmatic rocks.

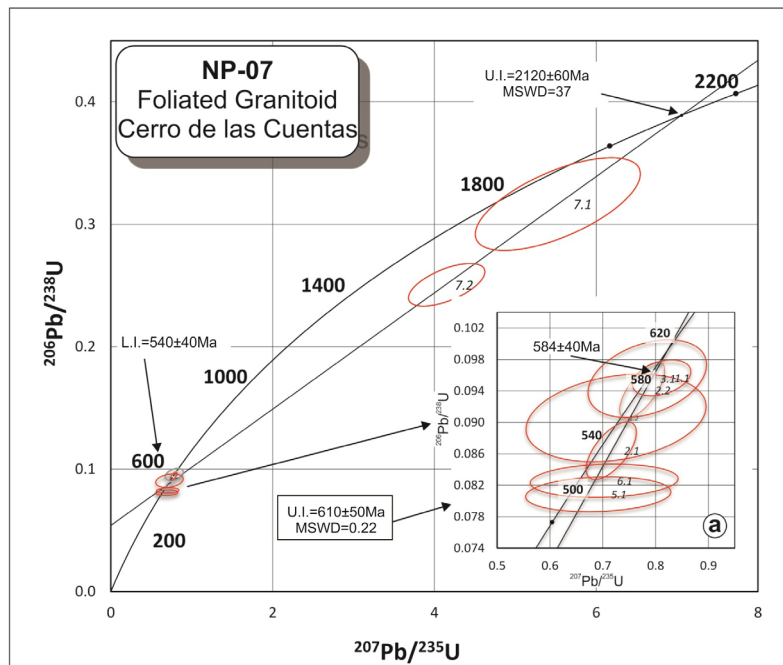


FIG. 6. U-Pb SHRIMP Concordia Diagram for the Cerro de las Cuentas granite (NP-07); a) ellipses indicate the analyses used for the age calculation. Error ellipses are at 95% confidence level.

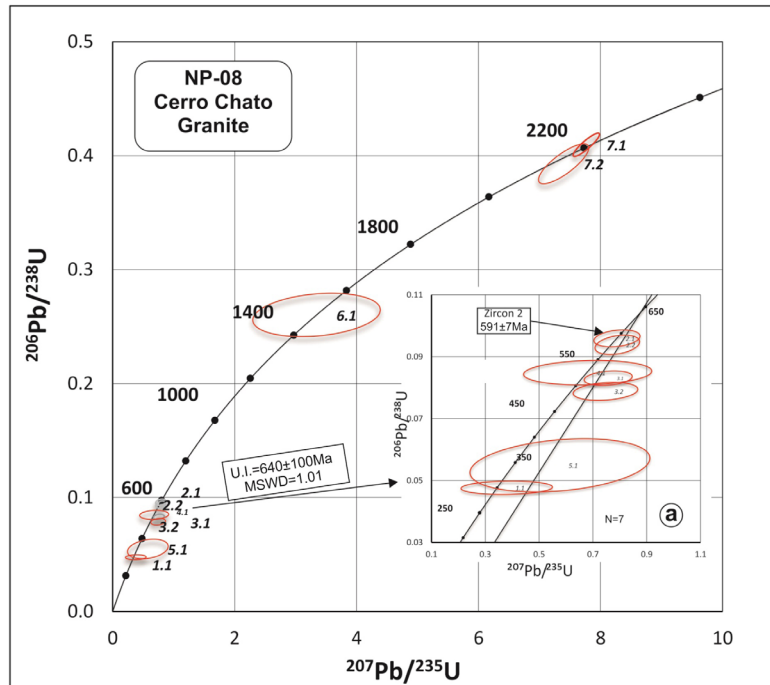


FIG. 7. U-Pb SHRIMP Concordia Diagram for the Cerro Chato granite (NP-08); a) ellipses indicate the analyses used for the age calculation. Error ellipses are at 95% confidence level.

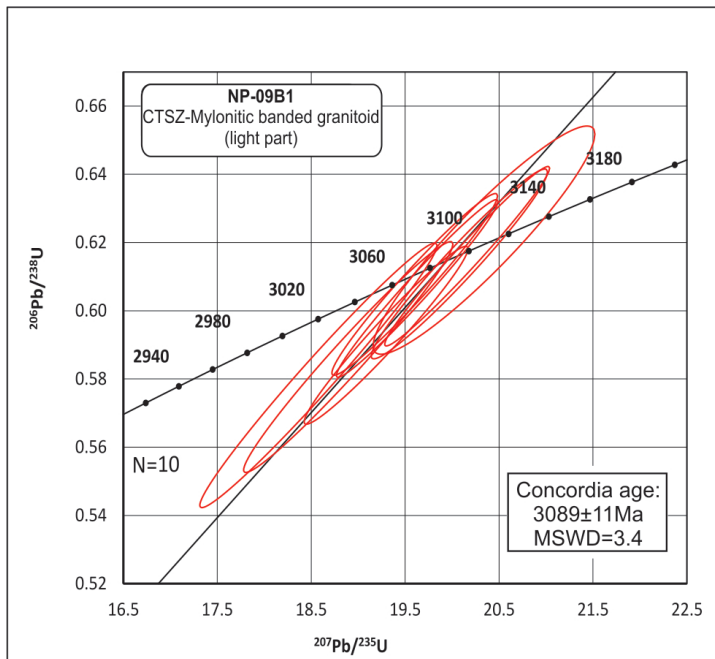


FIG. 8. U-Pb SHRIMP Concordia Diagram for Mylonitic granite from Cueva del Tigre shear zone (NP-09B1); ellipses indicate the analyses used for the age calculation. Error ellipses are at 95% confidence level.

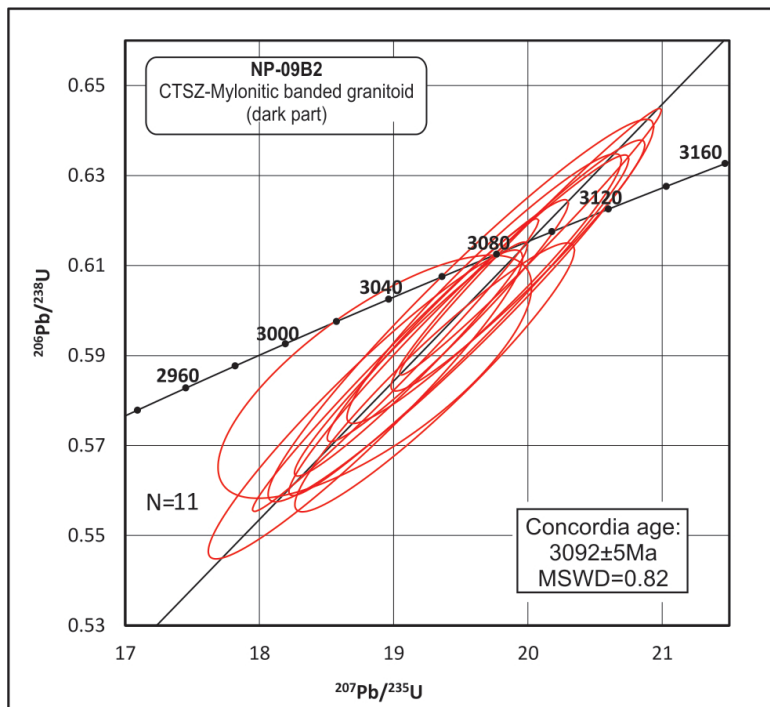


FIG. 9. U-Pb SHRIMP Concordia Diagram for Mylonitic granite from Cueva del Tigre shear zone (NP-09B2); ellipses indicate the analyses used for the age calculation. Error ellipses are at 95% confidence level.

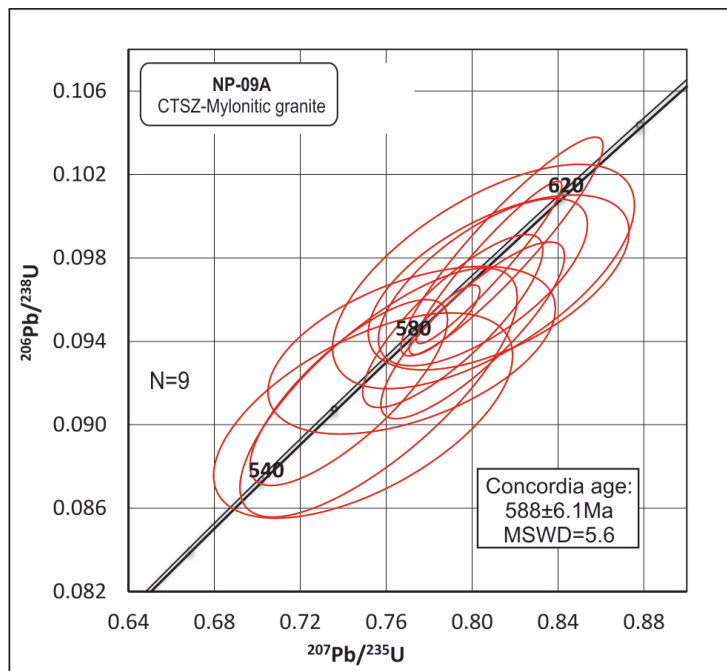


FIG. 10. U-Pb SHRIMP Concordia Diagram for Mylonitic granite form Cueva del Tigre shear zone (NP-09A); ellipses indicate the analyses used for the age calculation. Error ellipses are at 95% confidence level.

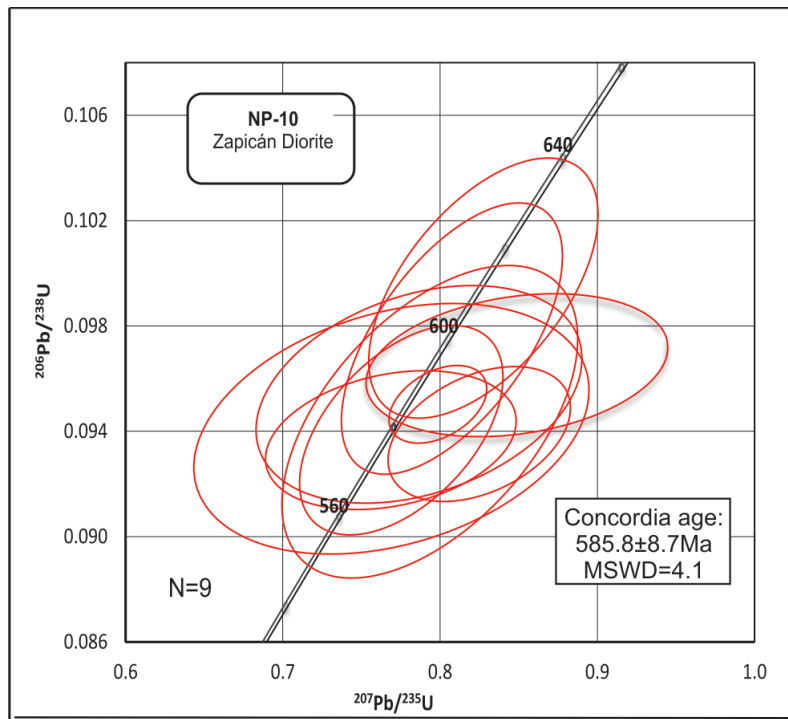


FIG. 11. U-Pb SHRIMP Concordia Diagram for La China Complex (NP-10); ellipses indicate the analyses used for the age calculation. Error ellipses are at 95% confidence level.

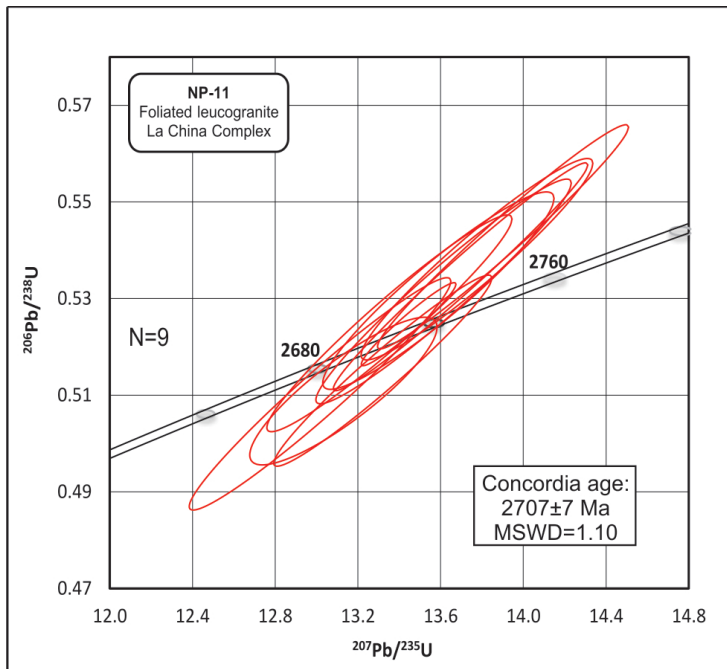


FIG. 12. U-Pb SHRIMP Concordia Diagram for La China Complex (NP-11); ellipses indicate the analyses used for the age calculation. Error ellipses are at 95% confidence level.

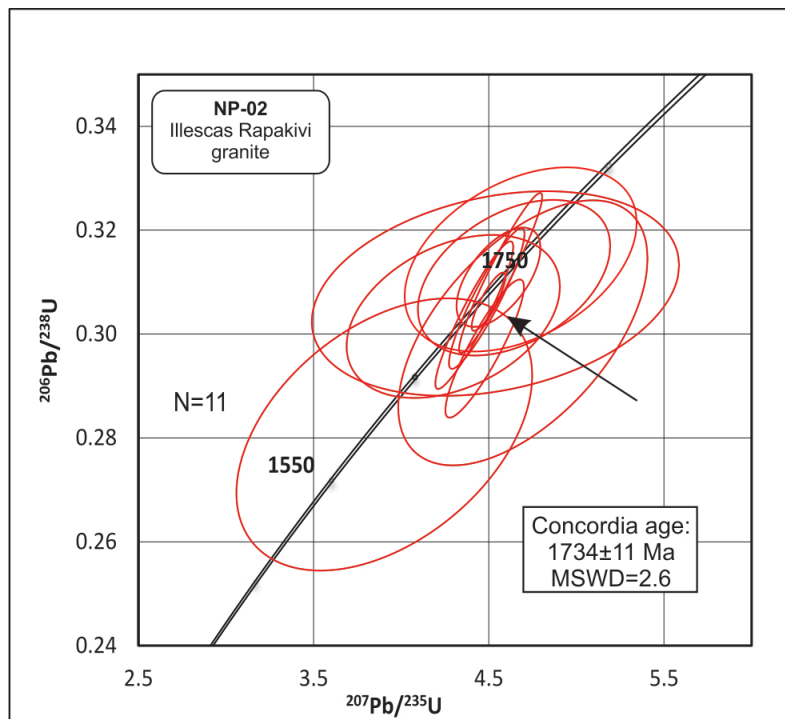


FIG. 13. U-Pb SHRIMP Concordia Diagram for Illescas rapakivi granite (NP-02); ellipses indicate the analyses used for the age calculation. Error ellipses are at 95% confidence level.

Zircon grains in samples NP-09B1 and NP-09B2 are also prismatic with oscillatory zoning cut off by areas of re-homogenization and with Th/U ratios between 0.17 to 0.70. Eight grains of the NP-09B1 sample yielded a concordant age of 3089 ± 11 Ma (10 spots) (Fig. 8). In the case of sample NP-09B2, 16 spots were measured in 12 zircon crystals. A concordant age of 3092 ± 5 Ma (Fig. 9) were obtained from 11 out of 16 spots (highly discordant data was discarded). Both samples show almost identical ages interpreted here as the crystallization age.

4.4. Sample NP-10-Deformed Zapicán diorite

This sample was also collected close to the Cueva del Tigre shear zone, not far from outcrop NP-09 (Fig. 2). The rock corresponds to the Zapicán diorite, composed by plagioclase+amphibole (+quartz+K-feldspar+biotite). It is locally foliated, presenting some bulging recrystallization and undulose extinction in quartz crystals.

Eleven zircon crystals were analyzed (Table 2). Zircon grains are generally prismatic with oscillatory zoning; also, some grains contain areas of re-homogenization and local recrystallization (Fig. 5). Th/U ratios of the analyzed zircon grains range from 0.71 to 1.61. Nine out of twelve spots were concordant and produced a very robust age of 585.8 ± 8.7 Ma (Fig. 11) interpreted as the time of rock crystallization.

4.5. Sample NP-11-Foliated leucogranite of the La China Complex

This sample was collected in the southern exposure of the La China Complex and corresponds to a foliated biotitic leucogranite (Fig. 2). Petrographically, it is made up of plagioclase, quartz and perthitic microcline as the predominant minerals, muscovite and biotite are arranged parallel to the foliation.

Zircon grains are generally prismatic, stubby, with areas of re-homogenization (Fig. 5) and contain Th/U ratios between 0.07 and 0.62. Twelve spots from eleven zircon crystals were analyzed yielding a concordant age of 2707 ± 7 Ma (Fig. 12) interpreted as the crystallization age.

4.6. Sample NP-02-Illescas rapakivi granite

The analyzed sample was collected in the central part of the Illescas rapakivi granite (Fig. 2)

and corresponds to an inequigranular, medium grained granitoid, composed of quartz+K-feldspar \pm plagioclase \pm amphibole \pm biotite \pm titanite \pm zircon \pm apatite. Deformation (undulose extinction and bulging recrystallization) is observed in quartz and K-feldspars, and perthites are present. Profuse sericitic alteration is observed.

Twelve zircon crystals were analyzed, being prismatic, either dark or light, with oscillatory zoning, and Th/U ratios from 1.10 to 2.40. Eleven concordant spots yielded a robust age of 1734 ± 11 Ma, shown in figure 13, and interpreted as the crystallization age.

5. Discussion

5.1. Archean ages in the Nico Pérez Terrane

When considering the whole geochronologic data, both old and new data presented here, relevant improvements for the understanding of the tectonic evolution of the Nico Pérez Terrane are achieved. Archean age of metaigneous rocks from the Pavas Block, formerly reported by Hartmann *et al.* (2001), was confirmed by three samples of La China Complex. Two of them are from a mylonitic granite (NP-09B) affected by the Cueva del Tigre shear zone. These samples show Mesoarchean ages whose results are identical within experimental error (NP-09B1= $3,089 \pm 11$ Ma and NP-09B2= 3092 ± 5 Ma), suggesting a magmatic event at that time. The third sample from Pavas Block is a foliated leucogranite yielding an age of 2707 ± 7 Ma assumed as magmatic. Thus, the ages of magmatism (*ca.* 3-2.7 Ga; Table 1) and metamorphism (*ca.* 2.7 Ga; Table 1) reported by different authors (Hartmann *et al.*, 2001; Gaucher *et al.*, 2014a; and references therein), as well as those carried out in this study, can be gathered into two groups: Mesoarchean and Neoarchean.

Moreover, the detrital zircon grain ages reported in the literature for Las Tetas Complex and Valentines-Rivera Granulitic Complex (Valentines Formation), suggest the existence of Paleo to Mesoarchean source areas. This is also supported by Lu-Hf data obtained by Oriolo *et al.* (2016a) for this area. The age of 3.4 Ga reported by Hartmann *et al.* (2001) could correspond to a Paleoarchaeon crust. Then, in tectonomagmatic events around 3.1 Ga formed the tonalitic rocks and around 2.7 Ga occurred magmatism and metamorphism

at medium-high grade (Hartmann *et al.*, 2001; Gaucher *et al.*, 2011).

5.2. The Illescas Batholith: tectonic significance

The robust U-Pb Statherian zircon age of 1734 ± 11 Ma obtained here for the Illescas Batholith, which is intrusive into the western part of the Valentines Block, is very similar to the ages indicated previously by Bossi and Campal (1992), Campal and Schipilov (1995) and Oriolo *et al.* (2019). This batholith has been considered related to an extensional episode within the Nico Pérez Terrane, possibly genetically coeval with the extensional event that originated the important Florida dike swarm in the Piedra Alta Terrane located immediately west of the Sarandí del Yí shear zone (Gaucher and Blanco, 2014). In this framework, the Illescas Batholith and the Florida dike swarm could represent the break-up or widespread extension of the Atlantica supercontinent or the Statherian taphrogenic episode (Brito Neves *et al.*, 1995; Gaucher and Blanco, 2014). The Sarandí del Yí shear zone, is located between these two units, along which some horizontal displacement may have taken place (Bossi and Campal, 1992).

Scarce and incomplete set of geochemical data (only two samples) for the Illescas Batholith presented by Gaucher and Blanco (2014) indicate a within plate anorogenic environment. However, Oriolo *et al.* (2019) based on a complete set of geochemical data (seven samples), suggested a post-collisional/post-orogenic setting. According to the available ages for the Nico Pérez Terrane, this suggestion is debatable, since the previous recorded orogenic event happened *ca.* 200 Ma before. Therefore, the most realistic hypothesis is an anorogenic setting. In addition, the alkali-calcic signature mentioned by Oriolo *et al.* (2019) could be related to typical crustal contamination.

5.3. Neoproterozoic magmatism in the Nico Pérez Terrane

Neoproterozoic crystallization ages are recorded in four intrusive granitoids in Valentines-Rivera Granulitic Complex and in La China Complex. The mylonitic granite (sample NP-09A) affected by Cueva del Tigre shear zone, yielded an Ediacaran age of 588 ± 6.1 Ma. This sample contains an inherited zircon crystal with a xenocrystal core of 3089 ± 13 Ma,

identical to the neighbor sample NP-09B. This feature also suggests a Mesoarchean age for the protolith of this unit. In addition, it is confirmed the Ediacaran age for the Zapicán diorite (585.8 ± 5.7), even though it is younger than the previous report made by Oriolo *et al.* (2016a) of 610 ± 2.5 Ma.

In the Valentines Block, a few Rhyacian inherited zircon xenocrystals with ages between 2200 and 2100 Ma were obtained in Cerro de Las Cuentas and Cerro Chato Ediacaran granitic plutons (NP-07 and NP-08, respectively). This evidence confirms previous ages obtained by Santos *et al.* (2003, 2017) and Oriolo *et al.* (2016a) for the widespread Paleoproterozoic basement rocks. Hence, the obtained results of our work confirm the post-orogenic Ediacaran magmatism that affected both the Valentines and Pavas blocks. These Ediacaran ages are comparable with several data reported in the literature for the Nico Pérez Terrane and the Dom Feliciano Belt (Mallmann *et al.*, 2007; Sánchez Bettucci *et al.*, 2010b; Oriolo *et al.*, 2016a).

The widespread granitoid magmatism of Neoproterozoic age (see Fig. 2) was coupled with the marked structural NE-SW shearing trend (Preciozzi *et al.*, 1979; Sánchez Bettucci *et al.*, 2010b). This structural feature affected the entire terrane and caused important disturbances, as shown by multiple shear zones, mylonitic features and regional foliation (Sánchez Bettucci *et al.*, 2010b). A good example is the Cueva del Tigre shear zone, represented by a group of granitic mylonites, schists and phyllonites at the boundary between the Valentines Block and La China Complex (Hartmann *et al.*, 2001). In addition, extensional tectonics may have been the cause of the formation of restricted sedimentary basins affected by low grade metamorphism over the Valentines Block, such as the meta-sandstones and meta-subarkoses of the Cerro San Francisco Formation and the oolitic and stromatolitic meta-limestones of the Cerros Victoria Formation (Montaña and Sprechmann, 1993), during Neoproterozoic times.

The intrusion of the granitic plutons can be attributed to the influence of the long-term tectono-magmatic episode related to the Brasiliano orogenic cycle. The field work carried out during sampling, allows the recognition of the Retamosa thrust as the eastern limit of the Nico Pérez Terrane against the Dom Feliciano supracrustal sequences (Figs. 1 and 2). This thrust is characterized by NNE general orientation with ESE vergence, being cut

in the southern portion by a NS normal fault. In the hanging wall Neoproterozoic supracrustal rocks outcrop.

5.4. Cratonic affinity of the Nico Pérez Terrane

The relative interaction between the Piedra Alta Terrane and the Nico Pérez Terrane (Fig. 1) has been interpreted in two different ways. According to Mallmann *et al.* (2007), Sánchez Bettucci *et al.* (2010a) and Santos *et al.* (2017, 2019) these terranes formed a coherent block, before the collision with the Kalahari Craton, when the Dom Feliciano Belt was formed. Therefore, the Nico Pérez Terrane would correspond to a reworked margin of the Río de la Plata Craton that was intensely deformed during the Brasiliano-Pan-African orogeny and adopted the NNE regional structural trend of the Dom Feliciano Belt. On the other hand, Oyhantçabal *et al.* (2011) challenged the Nico Pérez Terrane affinity with the Río de la Plata Craton based on lithologic, structural, geochronologic, and isotopic data. Oriolo *et al.* (2016a) and Oyhantçabal *et al.* (2018) suggested that the Nico Pérez Terrane would be an allochthonous crustal segment, originally part of the Congo Craton, that was accreted to the east (currently coordinates) of Piedra Alta Terrane along the Sarandí del Yí shear zone in Ediacaran times. Although interesting, this proposal is still an unfinished debate.

According to Dragone *et al.* (2017), the Congo Craton presents negative gravity bouguer anomalies whereas the Río de la Plata Craton, including Nico Pérez Terrane, have positive bouguer anomalies suggesting distinct lithosphere. Also, these authors mentioned that Congo Craton has crustal thicknesses above 40 km, while the Río de la Plata has a thinner and denser crustal thickness around 35 km. Furthermore, Bologna *et al.* (2019) based on magnetotelluric data concluded that no lithospheric-scale contrast in the electrical resistivity between Valentines Block and Piedra Alta Terrane occurs across the Sarandí del Yí shear zone. In fact, Bologna *et al.* (2019) mentioned that the overall resistivity structures of the Valentines Block and Piedra Alta Terrane are similar. These authors also suggest these two units were already a single and stable tectonic unit probably since the Paleoproterozoic, inferring that the Sarandí del Yí shear zone should be relatively shallow. In addition, Bologna *et al.* (2019) suggested that Neoproterozoic magmatism might not affected the mantle root under

the Valentines Block, concluding that this block is an extension of the Río de La Plata Craton.

The Piedra Alta Terrane, at the core of the Río de La Plata Craton, presents partially different tectonic evolution, even though Archean ages were recently identified in some of its lithological units (Santos *et al.*, 2017). The influence of the Brasiliano orogenic cycle, which is widespread in the Nico Pérez Terrane, is also recorded in some units of the Piedra Alta Terrane (Río de La Plata Craton) according to Santos *et al.* (2017). Up to now, the only Ediacaran magmatic body in the Piedra Alta Terrane is the anorogenic La Paz granite, with an age of 587 Ma (Cingolani *et al.*, 2012).

In a general way, the mainly Rhyacian units of the Piedra Alta Terrane, located within Arroyo Grande and San José belts, were originated in a magmatic arc setting, where tonalites, trondhjemites and granites predominate (Sánchez Bettucci *et al.*, 2010a and references therein). Nevertheless, in the Valentines Block (Nico Pérez Terrane) Rhyacian ages are present being the different units strongly deformed and metamorphosed by the Brasiliano orogenic cycle. A similar relation is encountered to the north, within the Rivera Block.

The exposed crustal level at the present surface in the Piedra Alta Terrane and the Nico Pérez Terrane seems to be different, considering the presence of a great amount of granulitic rocks in the Nico Pérez Terrane. In contrast, high grade metamorphic rocks are restricted to the Arroyo los Alamos Unit in the Piedra alta Terrane (Oyhantçabal *et al.*, 2007), indicating a higher crustal level. A possibility to explain this difference could be to envisage local displacements along the Sarandí del Yí shear zone, which was certainly one of the main tectonic elements in the Ediacaran/Cambrian times (Oriolo *et al.*, 2016b). It could also correspond to a pre-collision feature. The Rhyacian development of the bulk of the Piedra Alta Terrane possibly sets an upper time limit for the beginning of its behavior as a fault zone. From that time, the Sarandí del Yí shear zone was probably acting at successive pulses. Another speculative scenario could have been a thrust displacement of the Nico Pérez Terrane over the Piedra Alta Terrane, in which the Nico Pérez Terrane was uplifted and a deeper cortical level is now exposed at the present surface. This is supported by the recent work of Bologna *et al.* (2019) where the crust and upper mantle high-resistivity show no

lithospheric-scale contrast across the Sarandí del Yí shear zone. This suggests local displacement, not affecting the upper mantle. Also, the preliminary results of Moho depth and Vp/Vs ratio presented by Rodríguez *et al.* (2019) using one station near Tacuarembó (Nico Pérez Terrane) and the other near Salto city (Piedra Alta Terrane) show similar depth for the Moho.

Another important correlation between the Piedra Alta Terrane and the Nico Pérez Terrane could be the Statherian extensional tectonic event suggested by the emplacement of the Illescas rapakivi granite intruding the Valentines Block and the widespread Florida dike swarm occupying a great part of the Piedra Alta Terrane. Dyke swarms are distinctive representatives of mafic igneous activity associated with major continental rifting/plume events (*e.g.*, Ernst and Buchan, 1997; Salminen *et al.*, 2019) and are frequently related with rapakivi granites, particularly in Precambrian times. These dyke swarms associated with rapakivi granites, of similar ages, are an important tool for performing paleogeographic reconstructions of supercontinents. In Fact, rapakivi magmatism presents a characteristic temporal distribution in the world that could be contemporaneous with the supercontinent cycles (Larin, 2009; Salminen *et al.*, 2019, and references therein).

The above mentioned evidence of reworking in the Nico Pérez Terrane could be indicative of a metacratonization in the sense of Abdelsalam *et al.* (2011), Liégeois *et al.* (2013), Santos *et al.* (2017, 2019) and Girelli *et al.* (2018), during the Neoproterozoic Brasiliano-Pan African orogenic cycle (Mallmann *et al.*, 2007; Sánchez Bettucci *et al.*, 2010b; Oriolo *et al.*, 2017; among others).

6. Conclusions

The Nico Pérez Terrane is made up of a mosaic of tectonic blocks with different sizes, comprising a variety of rocks with different age and geological history. Archean granitoids are present in the Pavas Block, limited to the west by Cueva del Tigre shear zone. This block is affected by greenschist to amphibolite facies metamorphism, recording multiple metamorphic episodes and deformation. For the Valentines and Rivera blocks, a similar structural situation occurs, but the predominant rocks are Rhyacian granulites.

The Brasiliano-Pan African orogenic cycle, responsible for the amalgamation of Gondwana, affected the Nico Pérez Terrane and produced tectono-thermal activity and strong reworking of its rocks.

Acknowledgements

We are grateful to F. Santos Fernandes, V. Camara Maurer, E. Abelenda for the support in the laboratory and fieldwork and A. Latorres for the english review. Financial support was received from the Fundação de Amparo à Pesquisa do Estado de São Paulo (FAPESP) through grant 2013/12754-0 to UGC. We would like to thank S. Oriolo and the anonymous reviewer for the rigorous and constructive comments and suggestions.

References

- Abdelsalam, M.; Gao, S.; Liégeois, J.P. 2011. Upper mantle structure of the Saharan Metacraton. *Journal of African Earth Sciences* 60: 328-336. doi: 10.1016/j.jafrearsci.2011.03.009.
- Almeida, F.F.M.; Amaral, G.; Cordani, U.G.; Kawashita, K. 1973. The Precambrian evolution of the South American cratonic margin, South of Amazonia. *In The Ocean Basins and Margins* (Nairn, A.C.M.; Kanes, W.H.; Stehli, F.G.; editors). Plenum: 411-446. New York. doi: 10.1007/978-1-4684-3030-1_11.
- Bologna, M.S.; Dragone, G.N.; Muzio, R.; Peel, E.; Núñez Demarco, P.; Ussami, N. 2019. Electrical structure of the lithosphere from Río de La Plata Craton to Paraná Basin: amalgamation of cratonic and re-fertilized lithospheres in SW Gondwanaland. *Tectonics* 38 (1): 77-94. doi: 10.1029/2018TC005148.
- Bossi, J.; Umpierre, M. 1969. La petrología del yacimiento de hierro del arroyo Valentines, Florida: Uruguay. *In Jornadas Argentinas de Geología*, No. 4, Actas 1: 20 p. Mendoza.
- Bossi, J.; Campal, N. 1987. Evidencias geológicas sobre la posible existencia de un núcleo cratónico de más de 2.000 Ma en el Noreste de Uruguay. *In Simposio Sur-Brasilero de Geología*, No. 3, Actas 2: 821-832. Curitiba.
- Bossi, J.; Campal, N. 1992. Magmatismo y tectónica transcurrente durante el Paleozoico inferior del Uruguay. *In Paleozoico Inferior de Ibero-América* (Gutiérrez, J.; Saavedra, J.; Rábano, I.; editors). Universidad de Extremadura: 343-356. Alicante.
- Bossi, J.; Gaucher, C. 2004. The Cuchilla Dionisio Terrane, Uruguay: An Allochthonous Block Accreted in the

- Cambrian to SW-Gondwana. *Gondwana Research* 7 (3): 661-674.
- Bossi, J.; Fernández, A.; Elizalde, G. 1965. Predevoniano en el Uruguay. *Boletín Facultad de Agronomía* 78: 1-83.
- Bossi, J.; Campal Gennari, N.; Preciozzi Porta, F.L. 1993. Predevoniano en el Uruguay: Parte I. Terreno Piedra Alta. Dirección Nacional de Minería y Geología: 50 p. Montevideo.
- Bossi, J.; Campal Gennari, N.; Ferrando, L.A.; Gancio, F.; Schipilov, A.; Montaña, J.R.; Morales, H.L.; Piñeyro, D.; Sprechmann Heidenreich, P.W. 1998. Carta geológica del Uruguay: a escala 1/500.000 (CD-room). Universidad de la República, Facultad de Agronomía. Montevideo.
- Bruto Neves, B.B.; De Sá, J.M.; Nilson, A.A.; Botelho, N. 1995. A tafrogênese estateriana nos blocos paleoproterozóicos da América do Sul e processos susequentes. *Geonomos* 5 (3): 1-21.
- Campal, N.; Schipilov, A. 1995. The Illescas bluish quartz rapakivi granite (Uruguay-South America): some geological features. In *Symposium of Rapakivi Granites and Related rocks. Proceedings*: 18-18. Belem.
- Choubert, G.; Faure-Muret, A. 1969. *Carte tectonique internationale de l'Afrique, scale 1:5,000,000. Association of African Geological Surveys (ASGA) and United Nations Educational Scientific Surveys. Cultural Organisations (UNESCO)*: 9 p.
- Cingolani, C.; Basei, M.; Bossi, J.; Piñeyro, D.; Uriz, N. 2012. U-Pb (LA-ICP-MS) Zircon Age of the La Paz Granite (Pando Belt, Uruguay): An Upper Neoproterozoic magmatic event in the Río de La Plata Craton, *In South American Symposium on Isotope Geology*, No. 8: p. 139. Medellín.
- Cordani, U.G.; Soliani Jr., E. 1990. Idades K-Ar e Rb/Sr das "Ilhas Cristalinas" de Rivera e Aceguá (Uruguai e Rio Grande do Sul) e seu enquadramento geotectônico regional. *Anais Academia Brasileira de Ciências* 62:145-156.
- Dinamige. 2016. Relevamiento Aerogeofísico de Magnetometría y Espectrometría de Rayos Gamma-Mapa Geofísico del Uruguay. Ministerio de Industria, Energía y Minería. <http://www.miem.gub.uy/mineria-y-geologia/mapa-geofisico> (last visited 08/05/2021).
- Dragone, G.N.; Ussami, N.; Gimenez, M.E.; Lince Klinger, F.G.; Chaves, C.A.M. 2017. Western Parana suture/shear zone and the limits of Rio Apa, Rio Tebicuary and Rio de la Plata cratons from gravity data. *Precambrian Research* 291: 162-177. doi: 10.1016/j.precamres.2017.01.029.
- Ellis de Luca, J.H. 1998. The precambrian supracrustal rocks of the Isla Cristalina de Rivera in northern Uruguay and their ore deposits. Ph.D. Thesis (Unpublished), University of Heidelberg: 196 p.
- Ernst, R.E.; Buchan, K.L. 1997. Giant radiating dyke swarms: their use in identifying pre-Mesozoic large igneous provinces and mantle plumes. *Geophysical Monograph, American Geophysical Union* 100: 297-334. doi: 10.1029/GM100p0297.
- Fragoso-César, A.R.S. 1980. O craton do Rio de la Plata e o cinturão Dom Feliciano no escudo Uruguaio-Sul-Riograndense. In *Congresso Brasileiro de Geologia, Anais*, No. 31, Actas: 2879-2882. Camboriú.
- Franceschinis, P.R.; Rapalini, A.E.; Sánchez Bettucci, L.; Dopico, C.M.; Milanese, F.N. 2019. Paleomagnetic confirmation of the "unorthodox" configuration of Atlantica between 2.1 and 2.0 Ga. *Precambrian Research* 334 (105447). doi: 10.1016/j.precamres.2019.105447.
- Gaucher, C. 2000. Sedimentology, Paleontology and stratigraphy of the Arroyo del Soldado Group (Vendian to Cambrian, Uruguay). *Beringeria* 26: 1-120.
- Gaucher, C.; Blanco, G. 2014. Batolito de Illescas. In *Geología del Uruguay. Tomo 1: Predevónico* (Bossi, J.; Gaucher, C.; editors). Universidad de la República: 209-214. Montevideo.
- Gaucher, C.; Chemale Jr., F.; Bossi, J.; Castiglioni, E.A. 2010a. Grupo Cebollatí, Terreno Nico Pérez: definición y edad. In *Congreso Uruguayo de Geología*, No. 6. Actas en CD. Minas.
- Gaucher, C.; Sial, A.N.; Halverson, G.F.; Frimmel, H.E. 2010b. The Neoproterozoic and Cambrian: a time of upheavals, extremes, and innovations. *Neoproterozoic-Cambrian Tectonics, Global Change and Evolution: a focus on southwestern Gondwana*. In *Developments in Precambrian Geology* (Gaucher, C.; Sial, A.N.; Halverson, G.P.; Frimmel, H.E.; editors): 16: 3-11.
- Gaucher, C.; Frei, R.; Chemale, F.; Frei, D.; Bossi, J.; Martínez, G.; Chiglino, L.; Cernuschi, F. 2011. Mesoproterozoic evolution of the Río de la Plata Craton in Uruguay: at the heart of Rodinia? *International Journal of Earth Sciences* 100 (2-3): 273-288.
- Gaucher, C.; Bossi, J.; Chemale Jr., F.; García, G.; Frei, R.; Frei, D. 2014a. Complejo La China: las rocas más antiguas del Uruguay. In *Geología del Uruguay-Tomo 1: Predevónico* (Bossi, J.; Gaucher, C.; editors). Universidad de la República: 141-154. Montevideo.
- Gaucher, C.; Bossi, J.; Samaniego, L.; Frei, R. 2014b. Complejo Tapes. In *Geología del Uruguay-Tomo 1: Predevónico* (Bossi, J.; Gaucher, C.; editors). Universidad de la República: 253-264. Montevideo.
- Girelli, T.J.; Chemale Jr., F.; Lavina, E.L.C.; Laux, J.H.; Bongiolo, E.M.; Lana, C. 2018. Granulite accretion

- to Río de La Plata Craton, based on zircon U-Pb-Hf isotopes: Tectonic implications for Columbia Supercontinent reconstruction. *Gondwana Research* 56: 105-118. doi: 10.1016/j.gr.2017.12.010.
- Gómez Rifas, C. 1989. Tectónica Cretácea en Uruguay. In Simposio Cretáceo de América Latina, IGCP 242: A319-325. Buenos Aires.
- Hartmann, L.A.; Leite, J.A.; McNaughton, N.J.; Santos, J.O.S. 1999. Deepest exposed crust of Brazil-SHRIMP establishes three events. *Geology* 27 (10): 947-950. doi:10.1130/0091-7613(1999)027<0947:DEC OBS>2.3.CO;2.
- Hartmann, L.A.; Campal, N.; Santos, J.O.S.; Mcnaughton, N.J.; Bossi, J.; Schipilov, A.; Lafon, J.M. 2001. Archean crust in the Río de La Plata craton, Uruguay-SHRIMP U-Pb zircon reconnaissance geochronology. *Journal of South American Earth Sciences* 14: 557-570. doi: 10.1016/S0895-9811(01)00055-4.
- Hurley, P.M.; De Almeida, F.F.M.; Melcher, G.C.; Cordani, U.G.; Rand, J.R.; Kawashita, K.; Vandoros, P.; Pinson Jr., W.H.; Fairbairn, H.W. 1967. Test of continental drift by comparison of radiometric ages. *Science* 157 (3788): 495-500. doi: 10.1126/science.157.3788.495.
- Larin, A.M. 2009. Rapakivi granites in the geological history of the earth. In Part 1, magmatic associations with rapakivi granites: age, geochemistry, and tectonic setting. *Stratigraphy and Geological Correlation* 17 (3): 235. doi: 10.1134/S0869593809030010.
- Liégeois, J.P.; Abdelsalam, M.G.; Ennih, N.; Ouabadi, A. 2013. Metacraton: nature, genesis and behavior. *Gondwana Research* 23 (1): 220-237. doi: 10.1016/j.gr.2012.02.016.
- Lossada, A.C.; Rapalini, A.E.; Sánchez Bettucci, L. 2014. Enjambre de diques básicos de Nico Pérez-Zapicán, Uruguay: evidencias radimétricas y paleomagnéticas sobre su edad. *Revista de la Asociación Geológica Argentina* 71 (3): 345-355.
- Loureiro, J. 2008. Mapa Geológico de la Isla Cristalina De Rivera. Internal report (Unpublished), Dirección Nacional de Minería y Geología: 1 p. Montevideo.
- Loureiro, J.; Silva, H.; Sánchez Bettucci, L. 2019. Mapa Geológico: El Arqueano en el Uruguay. *Revista Investigaciones* 2 (1): 28-35. Montevideo. https://www.miem.gub.uy/sites/default/files/a3_loureiro_arqueano.pdf (last visited 10/05/2021).
- Ludwig, K.R. 2009. SQUID 2: a user's manual. Berkeley Geochronology Center. Special Publication 5: 1-110.
- Mallmann, G.; Chemale Jr., F.; Ávila, J.N.; Kawashita, K.; Armstrong, R.A. 2007. Isotope geochemistry and geochronology of the Nico Pérez Terrane, Río de La Plata Craton, Uruguay. *Gondwana Research* 12: 489-508. doi: 10.1016/j.gr.2007.01.002.
- Masquelin, H. 2006. El escudo uruguayo. In *Cuencas Sedimentarias de Uruguay, geología, paleontología y recursos minerales: Paleozoico* (Ubilla, M.; Veroslavsky, G.; editors). Facultad de Ciencias, Dirac 3: 37-106. Montevideo.
- Masquelin, H.; Silva, H.; Sánchez Bettucci, L.; Núñez, P.; Pascual, S.; Muzio, R.; Peel, E.; Scaglia, F. 2017. Lithologies, structure and basement-cover relationships in the schist belt of the Dom Feliciano Belt in Uruguay. *Brazilian Journal of Geology* 47 (1): 21-42. doi: 10.1590/2317-4889201720160119.
- Massonne, H.J.; Tikovsky, T.; Hartmann, L.A. 2001. Petrology of the 2.0 Ga old Santa María Chico granulites in southern Rio Grande do Sul, Brazil, and implications for crustal thickening in Paleoproterozoic times. In *Congreso Latinoamericano de Geología*, No. 11, Actas en CD. Montevideo.
- Montaña, J.; Sprechmann, P. 1993. Calizas estromatolíticas y oolíticas en el Uruguay y definición de la Formación Arroyo de la Pedrera (Cámbrico medio-Caradociano). In *Simposio Internacional del Neoproterozoico-Cámbrico de la Cuenca del Plata*, No. 1, Actas 2: p. 53.
- Oriolo, S.; Oyhantçabal, P.; Basei, M.A.S.; Wemmer, K.; Siegesmund, S. 2016a. The Nico Pérez Terrane (Uruguay): From Archean crustal growth and connections with the Congo Craton to late Neoproterozoic accretion to the Río de La Plata Craton. *Precambrian Research* 280: 147-160. doi: 10.1016/j.precamres.2016.04.014.
- Oriolo, S.; Oyhantçabal, P.; Wemmer, K.; Basei, M.A.S.; Benowitz, J.; Pfänder, J.; Hannich, F.; Siegesmund, S. 2016b. Timing of deformation in the Sarandí del Yí Shear Zone, Uruguay: Implications for the amalgamation of western Gondwana during the Neoproterozoic Brasiliano-Pan-African Orogeny. *Tectonics* 35: 754-771. doi: 10.1002/2015TC004052.
- Oriolo, S.; Oyhantçabal, P.; Wemmer, K.; Siegesmund, S. 2017. Contemporaneous assembly of Western Gondwana and final Rodinia break-up: implications for the supercontinent cycle. *Geoscience Frontiers* 8 (6): 1431-1445.
- Oriolo, S.; Oyhantçabal, P.; Konopásek, J.; Basei, M.A.; Frei, R.; Sláma, J.; Wemmer, K.; Siegesmund, S. 2019. Late Paleoproterozoic and Mesoproterozoic magmatism of the Nico Pérez Terrane (Uruguay): Tightening up correlations in southwestern Gondwana. *Precambrian Research* 327: 296-313. doi: 10.1016/j.precamres.2019.04.012.

- Oyhantçabal, P.; Muzio, R.; De Souza, S. 1993. Geología y aspectos estructurales del borde orogénico en el extremo sur del cinturón Dom Feliciano. *Revista Brasileira de Geociências* 23 (3): 296-300.
- Oyhantçabal, P.; Spoturno, J.; Loureiro, J. 2007. Caracterización geológica de las rocas Paleoproterozoicas de la región Centro-Sur del Uruguay (Terreno Piedra Alta-Cratón del Río de La Plata). In *Congreso Uruguayo de Geología*, No. 5, Actas en CD. Montevideo.
- Oyhantçabal, P.; Siegesmund, S.; Wemmer, K. 2011. The Río de la Plata Craton: a review of units, boundaries, ages, and isotopic signature. *International Journal Earth Science (Geol Rundsch)* 100: 201-220. doi: 10.1007/s00531-010-0580-8.
- Oyhantçabal, P.; Wagner-Eimer, M.; Wemmer, K.; Schulz, B.; Frei, R.; Siegesmund, S. 2012. Paleo- and Neoproterozoic magmatic and tectonometamorphic evolution of the Isla Cristalina de Rivera (Nico Pérez Terrane, Uruguay). *Journal of South American Earth Sciences* 101: 1745-1762. doi: 10.1007/s00531-012-0757-4.
- Oyhantçabal, P.; Oriolo, S.; Philipp, R.P.; Wemmer, K.; Siegesmund, S. 2018. The Nico Pérez Terrane of Uruguay and Southeastern Brazil. In *Geology of Southwest Gondwana* (Siegesmund, S.; Basei, M.; Oyhantçabal, P.; Oriolo, S.; editors). Regional Geology Reviews, Springer: 161-188. doi: 10.1007/978-3-319-68920-3_7.
- Preciozzi, F.; Spoturno, J.; Heinzen, W. 1979. Carta geoestructural del Uruguay, escala 1/2.000.000. Ministerio de Industria y Energía, Instituto Geológico Ingeniero Eduardo Terra Arocena: 1-62. Montevideo.
- Preciozzi, F.; Spoturno, J.; Heinzen, W.; Rossi, P. 1985. Carta Geológica del Uruguay a escala 1:500.000. Texto explicativo. Ministerio de Industria y Energía, Dirección Nacional de Minería y Geología: 1-92. Montevideo.
- Rapela, C.W.; Pankhurst, R.J.; Casquet, C.; Fanning, C.M.; Baldo, E.G.; González-Casado, J.M.; Galindo, C.; Dahlquist, J. 2007. The Río de la Plata Craton and the assembly of SW Gondwana. *Earth-Science Reviews* 83: 49-82.
- Rodríguez, M.; Curbelo, A.; Castro, H.; Dell'Acqua, D.; Latorres, E.; Sánchez Bettucci, L.; Assumpção, M. 2019. Crustal thickness and vp/vs ratio for three stations in Uruguay using receiver function analysis: preliminary results. In *Simpósio Brasileiro de Sismologia*, No. 3: p. 87. San Pablo.
- Salminen, J.; Klein, R.; Mertanen, S. 2019. New rock magnetic and paleomagnetic results for the 1.64 Ga Suomenniemi dyke swarm, SE Finland. *Precambrian Research* 329: 195-210. doi: 10.1016/j.precamres.2018.01.001.
- Sánchez Bettucci, L.; Peel, E.; Oyhantçabal, P. 2010a. Precambrian geotectonic units of the Río de La Plata craton. *International Geology Review* 52 (1): 32-50. doi: 10.1080/0020681090321104.
- Sánchez Bettucci, L.; Peel, E.; Masquelin, H. 2010b. Neoproterozoic tectonic synthesis of Uruguay. *International Geology Review* 52 (1): 51-78. doi: 10.1080/00206810903358095.
- Santos, J.O.S.; Hartmann, L.A.; Bossi, J.; Campal, N.; Schipilov, A.; Piñeyro, D.; McNaughton, N.J. 2003. Duration of the Trans-Amazonian Cycle and its correlation within South America based on U-Pb SHRIMP geochronology of the La Plata Craton, Uruguay. *International Geology Review* 45: 27-48. doi: 10.2747/0020-6814.45.1.27.
- Santos, J.O.S.; Chernicoff, C.J.; Zappettini, E.O.; McNaughton, N.J.; Greau, Y. 2017. U-Pb geochronology of Martín García, Sola, and Dos Hermanas Islands (Argentina and Uruguay): Unveiling Rhyacian, Statherian, Ectasian, and Stenian of a forgotten area of the Río de la Plata Craton. *Journal of South American Earth Sciences* 80: 207-228.
- Santos, J.O.S.; Chernicoff, C.J.; Zappettini, E.O.; McNaughton, N.J.; Hartmann, L.A. 2019. Large geographic and temporal extensions of the Río de La Plata Craton, South America and its metacratonic eastern margin. *International Geology Review* 61 (1): 56-85. doi: 10.1080/00206814.2017.1405747.
- Sato, K.; Tassinari, C.; Basei, M.A.S.; Júnior, O.; Onoe, A.; Souza, M. 2014. Sensitive High Resolution Ion Microprobe (SHRIMP IIe/MC) of the Institute of Geosciences of the University of São Paulo, Brazil: Analytical method and first results. *Geologia USP. Série Científica* 14: 3-18. doi: 10.5327/Z1519-874X201400030001.
- Solian, E. 1986. Os dados geocronológicos do Escudo Sul-Rio Grandense e suas implicações de ordem geotectônica. Ph.D. Thesis (Unpublished), Universidade de São Paulo: 243 p.
- Williams, I.S. 1998. U-Th-Pb geochronology by ion microprobe. *Reviews in Economic Geology* 7: 1-35. doi: 10.5382/Rev.07.01.